nature portfolio

Peer Review File

Blood-Brain Barrier-Penetrant Nanotherapy Inhibits Haem Oxygenase-1-Mediated Ferroptosis for Post-Resuscitation Neuroprotection

Corresponding Author: Professor Jiajia Xiang

This file contains all reviewer reports in order by version, followed by all author rebuttals in order by version.

Version 0:

Reviewer comments:

Reviewer #1

(Remarks to the Author)
This study introduces a promising nanotherapeutic approach using OAMs to deliver artesunate across the BBB, effectively addressing the critical challenge of post-resuscitation neuroprotection in cardiac arrest research. The work stands out for its robust preclinical evidence, integrating the design of BBB-penetrant nanocarriers with novel mechanistic dissection of haem oxygenase-1 (HMOX1)-mediated ferroptosis in post-resuscitation neuronal death. Identification of the HMOX1-ferroptosis axis as a therapeutic target, coupled with the translational potential of OPDEA micelles, represents a notable advancement in the fields of CNS drug delivery and neuroprotective strategies. The manuscript is well-conceived, and the experimental design is rigorous. I recommend its publication once the following minor issues have been addressed:
1. As the HMOX1-ferroptosis pathway forms the conceptual core of this study, a more detailed discussion of the pathological implications of HMOX1 in ferroptosis within the Introduction section would enhance the narrative flow.
2. Figure 6 demonstrates HMOX1 upregulation at the transcriptomic level. Additional validation at the protein level (e.g., Western blot) in hippocampal tissue is necessary to substantiate these findings.
3. The CA/CPR model methodology should be further elaborated, including ECG criteria for arrest confirmation, exact procedural steps, and parameters used for CA induction and CPR, to ensure reproducibility. The dosing regimen should be clearly described in the Methods section.
4. For the TEM-based assessment of mitochondrial morphology, it is unclear whether the quantification was performed on a per-cell basis or per field of view. The authors should clarify how many cells or imaging fields were analysed per group, and what criteria were used for selecting those regions.
5. Is there any toxicity of OAMs to the main organs? The histologic examination, blood biochemistry, and blood routine tests are needed.
6. The study has demonstrated the BBB permeability of OAMs; however, a comparison of this platform with other BBB-crossing strategies, such as cell-penetrating peptides, in the Discussion section would help highlight its advantages and potential translational value.
7. Some formatting issues: capitalization in the Y-axis, e.g., Fig. 3, misalignment of the Y-axis in Fig. 9H.

Reviewer #2

(Remarks to the Author)
CA leads to global cerebral ischemia/reperfusion injury. Due to the existence of the BBB, there is currently a lack of effective therapies. In this study, the OAMs based on zwitterionic OPDEA micelles loaded with Art was developed, which can efficiently cross the BBB and accumulate in hippocampal neurons and microglia in a targeted manner. Through studies using in vitro hypoxia-reoxygenation and in vivo CA/CPR models, it was found that HMOX1 - mediated ferroptosis is the core mechanism of nerve cell death. OAMs can inhibit HMOX1, restore iron homeostasis, and reduce lipid peroxidation, thereby protecting mitochondrial function and neuronal survival. This study validates the HMOX1 - ferroptosis axis as a therapeutic target and also demonstrates the clinical translational potential of OPDEA micelles as a neuroprotective nano-platform. This study has certain innovation and significance, but it requires major revisions, including supplementing key experimental data, improving theoretical logic, and deepening the research.
1. The introduction section is not sufficiently in-depth and remains too superficial; it requires elaboration on the research background. For instance, a more detailed explanation of the specific molecular mechanisms underlying brain injury following cardiac arrest should be provided—moving beyond merely mentioning oxidative stress and neuroinflammation to

specifying which signaling pathways are activated. The discussion on ferroptosis and HMOX1 should also delve deeper into their molecular mechanisms, rather than simply referencing iron overload and lipid peroxidation. Key molecules such as GPX4 and System Xc- should be explicitly addressed. Additionally, the dual role of HMOX1 warrants a more thorough explanation, clarifying under what circumstances it acts protectively and when it becomes detrimental.
2. The TEM image of OAMs shows only two micelles in the entire field of view, which is too limited to assess whether the micelles are uniformly distributed. It is recommended to provide images with a larger field of view.
3. It is imperative to confirm the chemical structure of OAMs. Techniques such as ^{1}H NMR spectroscopy and FTIR should be employed to verify that the synthesized polymer is indeed OPDEA and to demonstrate successful drug encapsulation.
4. A more comprehensive evaluation of the stability of OAMs should be conducted. For example, both the stability and drug release profile of OAMs should be examined under different pH conditions. Moreover, in the paper, the in vitro release curve of Art was detected at room temperature. Why not conduct the detection at 37°C?
5. Does the transport of micelles across the blood-brain barrier and their subsequent accumulation in the brain are affected by I/R injury? Are there differences observed between healthy mice and those subjected to CA/CPR models?
6. Immunofluorescence staining of frozen sections using markers for endothelial cells (CD31), neurons (NeuN), and microglia (Iba1) did not reveal robust colocalization of OPDEA-Cy5PCL fluorescence with these three cell types. While these results indicate that the micelles can cross the BBB and reach brain tissue, they do not demonstrate specific accumulation within the aforementioned cell populations.
7. The text states that these micelles accumulate in the neurovascular unit and inflammatory cells; however, subsequent cellular experiments only examined endothelial cells and neurons. Why was the internalization of these micelles not investigated in microglia? It is recommended to supplement these experiments.
8. Experimental results demonstrate that the micelles within neuronal cells undergo rapid and efficient efflux (50.1% efflux at 3 hours, 60% at 6 hours). If the drug cannot accumulate effectively in neuronal cells, how can it exert subsequent therapeutic effects?
9. Neuroinflammation is primarily triggered by the activation of glial cells (microglia), and TNF-α and IL-1β are also predominantly produced by microglia. Therefore, merely detecting the expression of TNF-α and IL-1β in HT22 cells via qPCR does not sufficiently demonstrate that OAMs alleviate inflammatory signaling under H/R challenge.
10. The results of TUNEL staining and immunohistochemical staining for cleaved-caspase-3 are weak and fail to convincingly demonstrate the anti-apoptotic effects of OAMs. It is recommended to supplement these findings with Western blot experiments targeting key molecules involved in classical apoptotic pathways.
11. The article relies solely on measuring intracellular iron levels, lipid peroxidation, and GSH levels to establish the relationship between HMOX1 activity and the execution of ferroptosis in neurons, which is insufficiently comprehensive. It is necessary to supplement these data with WB analyses of key molecules involved in the classical ferroptosis pathway.
12. Why does overexpression of HMOX1 under normal conditions not activate ferroptosis, whereas under H/R conditions it exacerbates ferroptosis? It is recommended to supplement with further experiments to investigate the specific mechanism by which HMOX1 activates ferroptosis.
13. The production of mitochondrial reactive oxygen species is closely related to the mitochondrial membrane potential. Therefore, it is recommended to supplement the study with detection results of mitochondrial membrane potential under different conditions (e.g., JC-1 staining).
14. In the descriptions on lines 430 - 432 of the text, it is pointed out that the overexpression of HMOX1 abolished the cytoprotective effect of OAMs and re - induces ferroptosis in the cytoplasm and mitochondria. Then it is also stated that even in the case of HMOX1 overexpression, the combined treatment of OAMs largely restores the levels of ferroptosis markers. There is a contradiction between these two sentences, and it is recommended to make revisions.
15. The text mentions multiple times that micelles accumulate in microglia, and microglia are involved in I/R-induced brain injury. However, the entire article does not conduct research on OAMs in aspects such as microglia and neuroinflammation. Please supplement relevant experiments to make the article more substantial.
16. Some writing formats in the text are incorrect. When an abbreviation appears for the first time, the full name should be written. For example, in the Abstract section, the full name of CNS was not written when it first appeared. Please check and revise the entire text.
17. In the text, the dosage unit is sometimes written as μg/mL and sometimes as μg mL^{-1}. Please unify the writing according to the requirements.
18. Some pictures are not in standard format. For example, the description of the x-axis in Fig 2D is not aligned with the axis. Please check and revise the whole text.

Reviewer #3

(Remarks to the Author)
In this manuscript, Zhang et al. present a novel nanotherapeutic platform (OAMs) to mitigate post-resuscitation brain injury. The platform enhances blood-brain barrier (BBB) penetration of artesunate using zwitterionic OPDEA micelles that facilitate adsorptive-mediated transcytosis. This receptor-independent mechanism represents a significant advance over conventional delivery methods. The neuroprotective efficacy of OAMs was validated through comprehensive assessments in a murine CA/CPR model. Furthermore, the study elucidates a key molecular mechanism, demonstrating that OAMs exert their therapeutic effect by inhibiting heme oxygenase-1 (HMOX1)-mediated ferroptosis.
However, several concerns need to be addressed before the manuscript can be accepted for publication.
Concerns
1. In Figure 1B, please label the pink cells located within the blood vessel.
2. Figure S1B is not referenced in the results section.
3. Please clarify how it was determined that OAMs substantially prolonged drug circulation, and explain the calculation that shows 34.3% of the dose was retained at the specified time point.

4. Please check the time label in Figure 2D.
5. In Figures 3A and 3B, the β-actin and Cy5 staining is difficult to discern due to poor image resolution and the low density of the bEnd.3 and HT22 cells.
6. The resolution of Figure 3K is poor. Please provide a higher-resolution version.
7. In Figures 4D i and 4D ii, the cell counts in the flow cytometry plots are too small to read. Please enlarge them. In the legend for Figure 4, please define the symbols (*, #, †) used in the bar chart. Annexin-V staining detects apoptosis, whereas this study focuses on ferroptosis. The authors are suggested use a different method to assess cell viability, such as a WST assay.
8. To ensure a more direct and accurate comparison for the IHC staining in Figure 5E, tissue sections should be taken from the same or adjacent regions.
9. Although HMOX1 overexpression (oeHMOX1) enhances H/R-induced ferroptosis (Figure 7A), the data also show that oeHMOX1 alone did not elevate Fe2+ levels, whereas H/R stress did (Figures 7B-7J). This suggests that H/R stress promotes ferroptosis through additional mechanisms independent of HMOX1. Furthermore, while HMOX1 knockdown significantly ameliorated H/R-induced ROS generation and lipid peroxidation, it remains unclear if it can also rescue H/R-inhibited cell viability. I suggest that the authors investigate this. As a control, they should also test whether ferrostatin-1 can inhibit ferroptotic activity and improve the viability of HT22 cells subjected to H/R stress alone, which would also confirm the role of ferroptosis in H/R.
10. Based on the western blots in Figure S6A, the knockdown efficiency is not clear. Please provide quantification of the blot results. In Figure S6, RSL3 was applied to HT22 cells in vitro. Therefore, the dose should be reported in units of concentration (e.g., μM, nM) rather than mg/kg, which is an in vivo dosage unit.
11. Regarding lines 397-399, the authors state that RSL3 treatment reverses the protective effect of HMOX1 shRNA, thereby confirming the role of HMOX1. This reasoning is questionable because RSL3 is a direct inducer of ferroptosis. Furthermore, a control group showing the effect of RSL3 alone is missing and should be included.
12. Do H/R and CPR increase the protein expression of HMOX1? Does OAM treatment decrease HMOX1 expression? What is the potential mechanism for upregulating HMOX1?
13. In lines 430-431, the authors claim that HMOX1 overexpression "abolished" the cytoprotective effects of OAMs. However, while the data in Figures 8B-F show a statistically significant effect, the actual degree of rescue is minor. This suggests that OAMs have other protective mechanisms besides their effect on HMOX1, so the term "abolished" is an overstatement.
14. In Figure 9A, treatment with the HMOX1 activator CoPPIX-Cl appears to reverse the therapeutic benefits of OAMs. To confirm the pathological role of increased HMOX1, I suggest the authors test whether an HMOX1 inhibitor (e.g., Zinc Protoporphyrin) can attenuate CPR alone-induced neuronal injury.
15. For the ROS staining shown in Figure 9Eiii, images should be taken from the same or adjacent tissue regions to ensure a valid comparison.
16. Please ensure that all instances of "in vitro", "in vivo", and "ex vivo" are italicized throughout the manuscript.
17. In line 680, please state the pore size and catalog number of the transwell insert used for the trans-endothelial transport analysis.
18. The immediate administration of the nanotherapy does not reflect clinical practice, where treatment is typically delayed. To address this, I suggest performing experiments where the OAMs are administered at progressively later time points after successful CPR to determine how long the therapy remains effective.
19. The manuscript's primary focus on HMOX1-mediated ferroptosis overlooks the fact that artesunate has broad antioxidant capabilities. The specificity of its action against HMOX1 is not fully established, meaning off-target effects could contribute to the therapeutic outcome. The manuscript must be revised to differentiate the neuroprotective effects of specific HMOX1 inhibition from the compound's other biological activities.
20. The study confirmed the nanoparticles accumulate in neurons and microglia. Expanding the investigation to include their effects on other crucial brain cells such as astrocytes, oligodendrocytes, and pericytes would provide a more complete understanding of the therapy's impact on the entire neurovascular unit and overall brain environment.
21. The study focuses on artesunate as the encapsulated drug, which limits generalizability of the delivery platform to other potential neurotherapeutics. More data on versatility might have strengthened the case for OPDEA micelles as a general nanocarrier.

Version 1:

Reviewer comments:

Reviewer #1

(Remarks to the Author)
I have read through the revised manuscript and the response letter. All my concerns have been well addressed and therefore I would recommend publication of the manuscript on Nature communications.

Reviewer #2

(Remarks to the Author)
The author has systematically responded to and revised the manuscript based on the reviewers' comments, significantly improving the rigor of the experimental design, the completeness of the mechanism derivation, and the standardization of the expression. The current version of the study has a novel concept. It achieves the penetration of the BBB by Art through

OPDEA-based micellar carriers (OAMs) and targets the inhibition of HMOX1-mediated ferroptosis, providing an innovative and translation-potential treatment strategy for postiac-CA resuscitation brain injury. The research design is logically clear, the in vitro and in vivo data chains are basically complete, and the core conclusions are effectively supported. it has reached the publication level of the journal, and it is recommended to accept it after minor revisions.
1. The authors only detected the neuroprotective effect and acute toxicity within 24 hours, without evaluating the long-term (e.g., 1 week, 4 weeks) neurological function recovery and the safety of long-term HMOX1 inhibition. Considering the requirements of clinical translation, it is recommended to supplement the long-term safety data or clearly state the limitations of the short-term experiment in the discussion.
2. It is recommended to polish the language of the article and simplify the long and complex sentences.

Reviewer #3

(Remarks to the Author)
The authors have addressed my questions, and I have no further inquiries.

Version 2:

Reviewer comments:

Reviewer #2

(Remarks to the Author)
The author has fully responded to and implemented all the reviewers' comments, comprehensively improving the experimental design, data analysis, and conclusion interpretation. Currently, the article has clear logic, solid data, and sufficient arguments. It also has significant academic value and innovation, meeting the requirements of our journal for originality, rigor, and wide influence. It is recommended to accept the article for formal publication in Nature Communications.

RESPONSES TO REVIEWERS' COMMENTS

Title: Blood-brain barrier-penetrant nanotherapy inhibits HMOX1-mediated ferroptosis for post-resuscitation neuroprotection

Authors: Mao Zhang, Wenbin Zhang, Qiuyu Wei, Lu He, Jinyu Zhu, Jiaying Chen, Youqing Shen, Jiajia Xiang & Jiefeng Xu

We would like to express our sincere gratitude to the reviewers for their helpful and constructive suggestions, which have greatly improved the revised version. We have carefully noted their comments and suggestions, conducted additional experiments, and revised our manuscript accordingly.

A point-by-point response to all reviewers' comments is given in blue color alongside the reviewers' comments below. The revisions in the revised manuscript are highlighted in blue color.

Reviewer #1

This study introduces a promising nanotherapeutic approach using OAMs to deliver artesunate across the BBB, effectively addressing the critical challenge of post-resuscitation neuroprotection in cardiac arrest research. The work stands out for its robust preclinical evidence, integrating the design of BBB-penetrant nanocarriers with novel mechanistic dissection of haem oxygenase-1 (HMOX1)-mediated ferroptosis in post-resuscitation neuronal death. Identification of the HMOX1-ferroptosis axis as a therapeutic target, coupled with the translational potential of OPDEA micelles, represents a notable advancement in the fields of CNS drug delivery and neuroprotective strategies. The manuscript is well-conceived, and the experimental design is rigorous. I recommend its publication once the following minor issues have been addressed:

Author's response: Thank you for your positive comments on our work. We appreciate

your recognition of the advances made in this study, its translational potential, and the rigor of the experimental design.

Comment 1: As the HMOX1-ferroptosis pathway forms the conceptual core of this study, a more detailed discussion of the pathological implications of HMOX1 in ferroptosis within the Introduction section would enhance the narrative flow.

Author's response: Thank you for your valuable suggestion. To improve conceptual continuity and better justify our focus on the HMOX1-ferroptosis axis, we have expanded the Introduction to elaborate on the pathological role of HMOX1 in ferroptosis. Specifically, we now state:

"Among ferroptosis regulators, haem oxygenase-1 (HMOX1) occupies a paradoxical position (Physiol. Rev. 2016, 96, 1449-1508; Nat. Commun. 2025, 16, 1212). Under physiological or mild oxidative conditions, transient HMOX1 induction protects cells by facilitating haem catabolism and maintaining redox homeostasis (Nat. Rev. Immunol. 2021, 21, 411-425). However, under prolonged pathological stress, sustained HMOX1 activation increases Fe^{2+} release, expands the labile iron pool, impairs System Xc^-–GPX4 activity, and accelerates ACSL4-driven lipid peroxidation, turning HMOX1 from an antioxidant into a key driver of ferroptosis (Mol Neurodegener,2021, 16, 16; Redox Biol. 2014, 2, 273-283)."

These descriptions have been incorporated into the Introduction section (Lines 69-75).

Comment 2: Figure 6 demonstrates HMOX1 upregulation at the transcriptomic level. Additional validation at the protein level (e.g., Western blot) in hippocampal tissue is necessary to substantiate these findings.

Author's response: Thank you for your helpful suggestion. To substantiate the transcriptomic data at the protein level, we have performed Western blot analyses of HMOX1 in HT22 cells treated with OAMs under hypoxia/reoxygenation (H/R) conditions for 24 h and hippocampal tissue from the cardiac arrest/cardiopulmonary resuscitation (CA/CPR) model at 24 h post-resuscitation, where OAMs were

administered immediately after return of spontaneous circulation (ROSC). As shown in Fig. 6h, i, HMOX1 expression is significantly upregulated in both the *in vitro* H/R setting and *in vivo* hippocampal samples after CA/CPR and is markedly reduced following OAM treatment.

These data and corresponding descriptions have been incorporated into the revised manuscript (Lines 480-486).

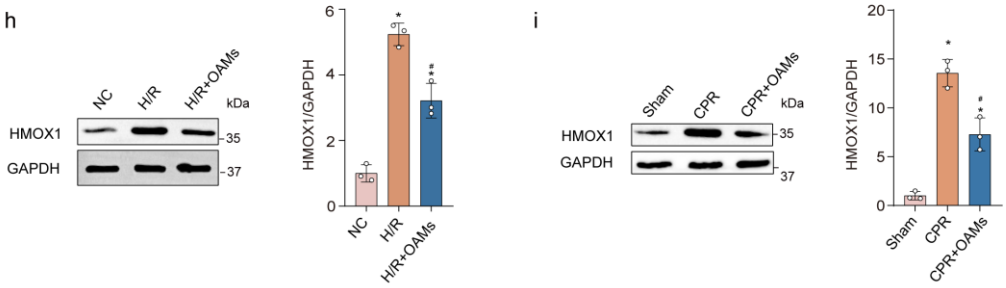

Fig. 6 h,i | h, Representative western blots (left) and quantification (right) of HMOX1 protein levels in HT22 cells under H/R with or without OAM treatment for 24 h ($n = 3$ biological replicates). Art-equivalent dose, 250 nM. **i**, Western blots (left) and relative expression levels (right) of HMOX1 in mouse hippocampal tissue 24 h after ROSC, following immediate post-ROSC administration of OAMs ($n = 3$ mice). Art-equivalent dose, 5 mg kg^{-1}. Data are presented as mean ± SD. Statistical significance was determined by one-way ANOVA with Tukey's post hoc test (multiple groups). $^{*}P < 0.05$ vs. NC or Sham; $^{\#}P < 0.05$ vs. H/R or CPR.

Comment 3: The CA/CPR model methodology should be further elaborated, including ECG criteria for arrest confirmation, exact procedural steps, and parameters used for CA induction and CPR, to ensure reproducibility. The dosing regimen should be clearly described in the Methods section.

Author's response: Thank you for this valuable comment. To ensure reproducibility and transparency, we have expanded the Materials and Methods to detail the CA/CPR model and the dosing schedules. Additionally, a schematic diagram has been included to further support experimental replication.

CA/CPR model methodology: We now provide explicit electrocardiogram (ECG)

criteria and stepwise procedures as follows:

"CA was induced by jugular i.v. injection of cold KCl (0.08 mg kg^{-1}), resulting in immediate asystole confirmed by a sustained flat ECG for 5 min. Resuscitation began after 5 min of arrest with ventilation, i.v. adrenaline (16 µg ml^{-1}, 100 µl), and chest compressions at 340–360 beats min^{-1}. Adrenaline was repeated every minute until ROSC or up to 10 min. ROSC is defined as sinus rhythm restoration with a mean arterial pressure (MAP) > 40 mm Hg and lasting ≥ 1 min. Ventilation continued at initial settings for 1 h post-ROSC, then with reduced tidal volume (0.7 ml) for another hour. Catheters were removed 2 h after resuscitation, and mice remained in a warming chamber until fully recovered before being returned to cages."

A representative ECG trace illustrating CA and ROSC has been added (Supplementary Fig. 8). Parameters, such as animal resuscitation time and cumulative epinephrine dose, are reported in Supplementary Tables 1,2,5,6 for each experiment. Experimental details have been incorporated into the revised manuscript (Lines 405-408; 791-800).

Dosing regimen: We now state all agents, routes, doses, and timings as follows:

"For in vivo studies, the following treatments were administered: Art or OAMs, single i.v. injection after ROSC (Art-equivalent dose, 5 mg kg^{-1}); CoPPIX-Cl, single i.v. injection after ROSC (10 mg kg^{-1}); ZnPP, single i.p. injection 24 h before CA induction (10 mg kg^{-1})."

A schematic timeline of CA induction, CPR, dosing, and outcome assessments is provided for clarity (Fig. 5a). These details have been incorporated into the revised manuscript (Lines 801-804).

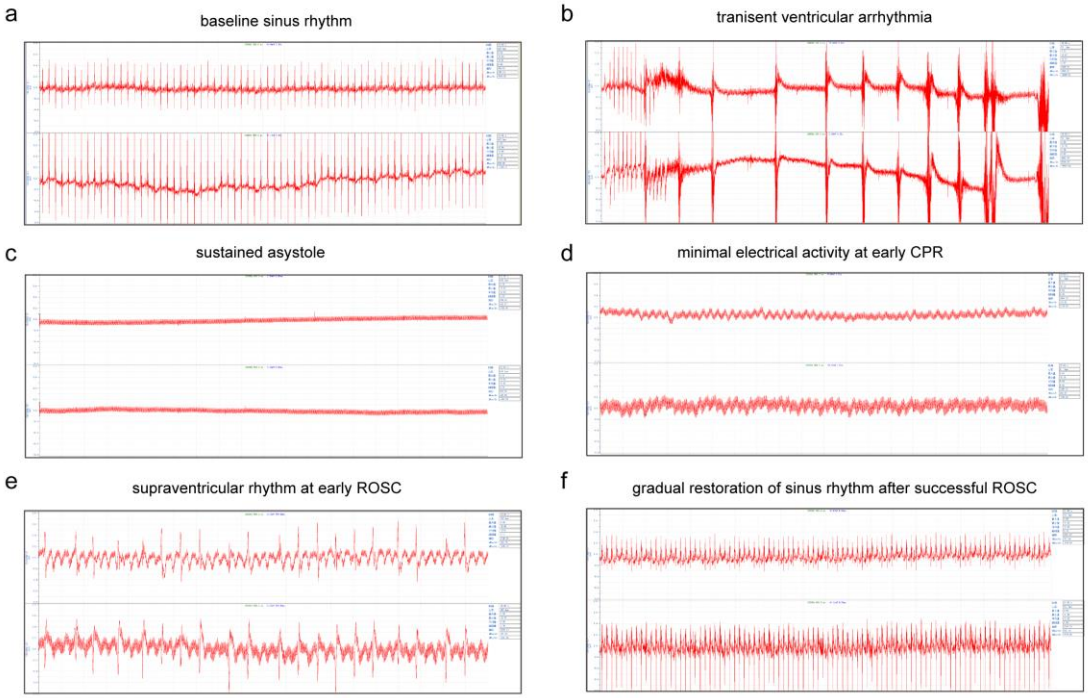

Supplementary Fig. 8 | ECG characteristics of the mouse CA/CPR model. Representative ECG traces illustrating the dynamic progression of the CA/CPR model: (**a**) baseline sinus rhythm; (**b**) tranisent ventricular arrhythmia; (**c**) sustained asystole; (**d**) minimal electrical activity at early CPR; (**e**) supraventricular rhythm at early ROSC; (**f**) gradual restoration of sinus rhythm after successful ROSC.

Supplementary Table 1. Baseline and CPR characteristics of mice in Fig. 5 (*n* = 6 mice).

Parameters	Sham	CPR	CPR+Art	CPR+OAMs	*P* value
Body weight, g	24.57±0.69	23.83±1.00	23.08±1.00	23.63±0.98	0.078
Heart rate, bpm	437.5±10.15	430.33±62.91	434.5±57.29	441.5±26.28	0.793
Body temperature, ℃	36.62±0.12	36.62±0.16	36.63±0.12	36.6±0.15	0.911
CPR time, min	/	4.00±0.89	5.33±1.21	4.17±1.47	0.172
Epinephrine dosage, μg	/	6.40±1.43	8.53±1.94	6.67±2.36	0.172

Note: "/" indicates that the measurement is not applicable to the Sham group, as no CPR procedure was performed. Art-equivalent dose, 5 mg kg^{-1}. Data are presented as

mean ± SD. Multi-group comparisons used one-way ANOVA for normally distributed data (Shapiro-Wilk test $P > 0.05$) or Kruskal-Wallis H test for non-normally distributed data (Shapiro-Wilk test $P \leq 0.05$), with $P < 0.05$ considered statistically significant.

Supplementary Table 2. Baseline and CPR characteristics of mice in Supplementary Fig. 9 (n = 3 mice).

Parameters	Sham	CPR	CPR+OAMs 30 min	CPR+OAMs 60 min	CPR+OAMs 120 min	*P* value
Body weight, g	24.43±0.47	24.13±0.80	24.47±0.50	24.6±0.46	24.3±0.17	0.840
Heart rate, bpm	390.67±2.08	392.00±35.55	379.33±5.03	407.33±23.16	403.33±11.727	0.479
Body temperature, ℃	36.6±0.10	36.67±0.15	35.6±1.56	36.63±0.12	36.6±0.35	0.363
CPR time, min	/	4.58±1.51	3.78±1.02	3.92±0.88	4.89±1.17	0.621
Epinephrine dosage, μg	/	8.00±1.60	6.40±1.60	6.40±1.60	8.00±1.60	0.441

Note: "/" indicates that the measurement is not applicable to the Sham group, as no CPR procedure was performed. Art-equivalent dose, 5 mg kg^{-1}. Data are presented as mean ± SD. Multi-group comparisons used one-way ANOVA or Kruskal-Wallis H test, with $P < 0.05$ considered statistically significant.

Supplementary Table 5. Baseline and CPR characteristics of mice in Fig. 10 (n = 8 mice).

Parameters	Sham	CPR	CPR+OAMs	CPR+OAMs+ CoPPIX-Cl	*P* value
Body weight, g	21.59±0.77	21.33±1.01	20.96±0.83	21.23±0.91	0.501
Heart rate, bpm	374.75±24.26	372.75±17.81	369.25±21.79	376.88±17.72	0.913
Body temperature, ℃	36.64±0.17	36.73±0.11	36.61±0.14	36.64±0.17	0.301
CPR time, min	/	3.56±0.73	3.69±0.86	3.88±1.02	0.801
Epinephrine dosage, μg	/	6.00±1.06	6.00±1.06	6.40±1.39	0.806

Note: "/" indicates that the measurement is not applicable to the Sham group, as no CPR procedure was performed. Art-equivalent dose, 5 mg kg^{-1}; CoPPIX-Cl-equivalent dose, 10 mg kg^{-1}. Data are presented as mean ± SD. Multi-group comparisons used one-way ANOVA or Kruskal-Wallis H test, with $P < 0.05$ considered statistically significant.

Supplementary Table 6. Baseline and CPR characteristics of mice in Supplementary Fig. 18 (*n* = 3 mice).

Parameters	Sham	CPR	CPR+ZnPP	*P* value
Body weight, g	24.47±0.38	24.17±0.25	24.00±0.78	0.581
Heart rate, bpm	386.67±7.64	391.00±26.89	414.00±22.52	0.295
Body temperature, ℃	36.50±0.00	36.53±0.06	36.63±0.12	0.154
CPR time, min	/	4.09±1.60	4.78±1.02	0.565
Epinephrine dosage, μg	/	6.93±2.44	8.53±0.92	0.349

Note: "/" indicates that the measurement is not applicable to the Sham group, as no CPR procedure was performed. ZnPP-equivalent dose, 10 mg kg^{-1}. Data are presented as mean ± SD. Differences between the two groups were analyzed using a two-tailed unpaired Student's *t* test or Mann-Whitney U test, and multi-group comparisons used one-way ANOVA or Kruskal-Wallis H test, with $P < 0.05$ considered statistically significant.

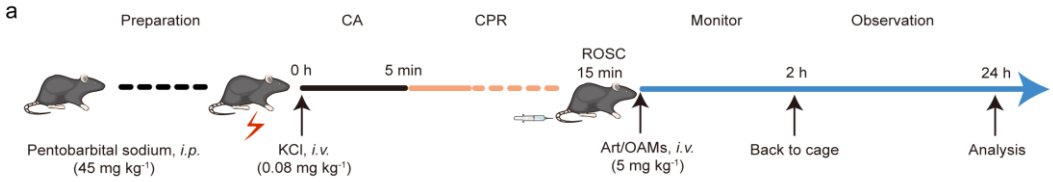

Fig. 5a | Schematic timeline of the CA/CPR procedure in C57BL/6 mice. After CA induction by *i.v.* KCl (0.08 mg kg^{-1}) at 0 h and maintained for 5 min, CPR was performed until ROSC or for up to 15 min, followed by *i.v.* administration of Art or

OAMs (5 mg kg^{-1}). All analyses were conducted 24 h after ROSC.

Comment 4: For the TEM-based assessment of mitochondrial morphology, it is unclear whether the quantification was performed on a per-cell basis or per field of view. The authors should clarify how many cells or imaging fields were analysed per group, and what criteria were used for selecting those regions.

Author's response: We appreciate the reviewer's helpful comment and have clarified the TEM quantification protocol in Materials and Methods to ensure reproducibility. For mitochondrial morphology, regions of interest (ROIs) were randomly selected based on: (i) intact cells with preserved cytoplasmic structure and (ii) absence of preparation artifacts. Mitochondrial morphology was quantified using ImageJ (Version 1.8.0). For each group, three independent biological replicates were analysed, with five independent fields per replicate. All identifiable mitochondria within each field were included. Two parameters were quantified: average cristae number per mitochondrion and the number of vacuolated mitochondria per field.

These details have been added to the revised manuscript (lines 997-1004).

Comment 5: Is there any toxicity of OAMs to the main organs? The histologic examination, blood biochemistry, and blood routine tests are needed.

Author's response: Thank you for raising this important point. To evaluate systemic safety, a comprehensive toxicity assessment of OAMs was carried out in healthy mice at an Art-equivalent dose of 5 mg kg^{-1}. At 24 h post-administration, histopathological examinations of main organs, blood routine tests, and serum biochemical analyses were performed. No tissue damage related to the treatment was detected, and the blood routine and biochemical parameters in OAM-treated mice showed no significant differences compared to the control group (Supplementary Fig. 10 and Supplementary Tables 3,4), indicating the excellent biosafety of OAM administration. The updated data and corresponding descriptions have been included in the revised manuscript (Lines 381-386).

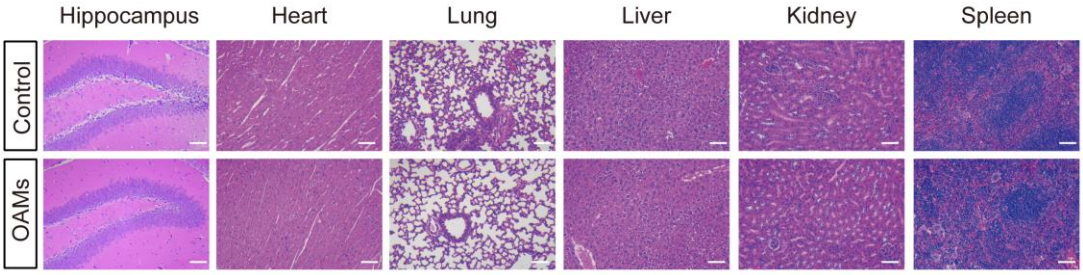

Supplementary Fig. 10 | Histological assessment of major organs following OAM administration. Haematoxylin and eosin (H&E) staining of hippocampus, heart, lung, liver, kidney, and spleen collected 24 h after *i.v.* administration of PBS (control) or OAMs (n = 3 mice). Art-equivalent dose, 5 mg kg^{-1}. Scale bars, 100 μm.

Supplementary Table 3. Blood routine parameters of C57BL/6 mice at 24 h after treatments.

Parameters	Control	OAMs	*P* value
WBC, $\times10^9$ L^{-1}	5.82±0.25	5.84±0.43	0.930
NEU, %	18.10±1.35	17.80±1.46	0.745
LY, %	64.18±6.28	66.67±2.94	0.447
RBC, $\times10^{12}$ L^{-1}	6.55±0.26	6.34±0.08	0.117
HGB, g L^{-1}	208.66±4.55	204.60±2.05	0.106
HCT, %	34.88±1.49	33.96±0.34	0.215
PLT, $\times10^9$ L^{-1}	308.80±35.57	319.40±37.41	0.658

Venous blood was collected at 24 h after administration from PBS (Control) and OAMs-treated mice for analysis (n = 5 mice; Art-equivalent dose, 5 mg kg^{-1}). Data are presented as mean ± SD. Differences between the two groups were analysed using two-tailed unpaired Student's t for normally distributed data or Mann-Whitney U test for non-normally distributed data, with $P < 0.05$ considered statistically significant. WBC, white blood cells; NEU, neutrophils; LY, lymphocytes; RBC, red blood cells; HGB, haemoglobin; HCT, haematocrit; PLT, platelets.

Supplementary Table 4. Biochemical parameters of C57BL/6 mice at 24 h after treatments.

Parameters	Control	OAMs	*P* value
NSE, ng ml^{-1}	1.49±0.33	1.68±0.36	0.420
cTN-I , pg ml^{-1}	23.48±3.02	26.17±3.25	0.213
SP-D, pg ml^{-1}	2.88±0.73	3.22±0.62	0.453
ALT, U l^{-1}	23.06±3.6	22.31±4.17	0.771
Cr, μmol l^{-1}	51.94±4.49	52.82±2.43	0.709

Plasma was collected at 24 h after administration from PBS (Control) and OAMs-treated mice for analysis (n = 5 mice; Art-equivalent dose, 5 mg kg^{-1}). Data are presented as mean ± SD. Differences between the two groups were analysed using two-tailed unpaired Student's t or Mann-Whitney U test, with $P < 0.05$ considered statistically significant. NSE (neuron-specific enolase) for brain injury; cTN-I (cardiac troponin I) for myocardial injury; SP-D (surfactant protein D) for lung injury; ALT (alanine aminotransferase) for hepatic injury; and Cr (creatinine) for renal injury.

Comment 6: The study has demonstrated the BBB permeability of OAMs; however, a comparison of this platform with other BBB-crossing strategies, such as cell-penetrating peptides, in the Discussion section would help highlight its advantages and potential translational value.

Author's response: Thank you for this valuable suggestion. We have included a comparison of OAMs and cell-penetrating peptides (CPPs) in the Discussion to better contextualise the advantages and translational potential of our BBB-penetrant platform.

CPPs, owing to their cationic nature and thus protein-adsorptive property, generally undergo rapid opsonisation and clearance (*Curr. Drug Targets, 2022, 23, 719-728*), resulting in a short systemic half-life and limited opportunity for BBB interaction In contrast, the zwitterionic OPDEA corona on OAMs provides ultra-low protein fouling and substantially prolongs circulation time (*Nat. Biomed. Eng., 2021, 5, 1019-1037*), a prerequisite for achieving sufficient BBB contact and subsequent transcytosis.

Mechanistically, CPP-mediated transport often depends on receptor- or transporter-mediated uptake, making its efficiency highly susceptible to pathological fluctuations in BBB protein expression (*ACS Mater. Lett., 2024, 6, 2239−2258*), which can cause variable BBB penetration across disease states. OAMs differ fundamentally in that they employ adsorptive-mediated transcytosis (AMT), driven by multiple hydrogen bonds between OPDEA and membrane phospholipids. This receptor-independent mechanism is more robust across diverse physiological and disease conditions, offering greater consistency and translational reliability. Finally, CPPs are highly effective at crossing individual cell membranes but do not inherently support the full transcellular trafficking necessary for BBB traversal, which involves coordinated vesicular transport from the luminal to the abluminal surface (*Adv. Drug Deliv. Rev., 2005, 57, 637-51*). OAMs, on the other hand, are designed to engage the entire AMT pathway, enabling complete transendothelial transport into the brain parenchyma, directly addressing the biological requirements for genuine BBB crossing.

These points have now been integrated into the Discussion to more clearly elucidate the mechanistic and translational advantages of OAMs relative to CPP-based strategies (Lines 738-741).

Comment 7: Some formatting issues: capitalization in the Y-axis, e.g., Fig. 3, misalignment of the Y-axis in Fig. 9H.

Author's response: Thank you for your feedback. We have corrected the Y-axis capitalisation in Fig. 3 and fixed the misalignment in Fig. 9h.

Reviewer #2

CA leads to global cerebral ischemia/reperfusion injury. Due to the existence of the BBB, there is currently a lack of effective therapies. In this study, the OAMs based on zwitterionic OPDEA micelles loaded with Art was developed, which can efficiently cross the BBB and accumulate in hippocampal neurons and microglia in a targeted manner. Through studies using in vitro hypoxia-reoxygenation and in vivo CA/CPR

models, it was found that HMOX1 - mediated ferroptosis is the core mechanism of nerve cell death. OAMs can inhibit HMOX1, restore iron homeostasis, and reduce lipid peroxidation, thereby protecting mitochondrial function and neuronal survival. This study validates the HMOX1 - ferroptosis axis as a therapeutic target and also demonstrates the clinical translational potential of OPDEA micelles as a neuroprotective nano-platform. This study has certain innovation and significance, but it requires major revisions, including supplementing key experimental data, improving theoretical logic, and deepening the research.

Author's response: Thank you very much for your positive evaluation of our work. We appreciate your recognition of the innovation, significance, and translational potential of this study.

Comment 1: The introduction section is not sufficiently in-depth and remains too superficial; it requires elaboration on the research background. For instance, a more detailed explanation of the specific molecular mechanisms underlying brain injury following cardiac arrest should be provided—moving beyond merely mentioning oxidative stress and neuroinflammation to specifying which signaling pathways are activated. The discussion on ferroptosis and HMOX1 should also delve deeper into their molecular mechanisms, rather than simply referencing iron overload and lipid peroxidation. Key molecules such as GPX4 and System Xc- should be explicitly addressed. Additionally, the dual role of HMOX1 warrants a more thorough explanation, clarifying under what circumstances it acts protectively and when it becomes detrimental.

Author's response: Thank you for these insightful and constructive suggestions. We agree that greater mechanistic depth in the Introduction is essential for motivating our study. In the revised manuscript, we have substantially expanded the background to provide a more detailed and pathway-specific overview of the molecular mechanisms underlying post-cardiac arrest (CA) brain injury.

First, the major injury pathways activated after global cerebral I/R include:

- Mitochondria-dependent apoptosis, driven by mitochondrial permeability

transition pore opening, release of cytochrome c and pro-apoptotic factors, and subsequent caspase activation *(Intensive Care Med., 2021, 47, 1393-1414)*.

- Excessive oxidative stress, resulting from impaired mitochondrial respiration and uncontrolled reactive oxygen species (ROS) generation, which triggers lipid, protein, and DNA damage and is exacerbated by Glutathione (GSH) depletion *(Biomaterials, 2024, 311, 122678)*.
- Neuroinflammation, mediated by NOD-like receptor family pyrin domain-containing 3 (NLRP3) inflammasome activation in microglia, leading to Caspase-1-dependent pyroptosis and release of pro-inflammatory cytokine, such as interleukin-1 beta (IL-1β) and interleukin-18 (IL-18) *(J. Neuroinflamm., 2020, 17, 219)*.

These additions clarify the upstream injury landscape within which ferroptosis emerges as an additional, but previously under-defined, mechanism.

Second, we enriched the description of ferroptosis by explaining the two core molecular axes that drive its execution:

- Antioxidant system failure, characterised by dysfunction of the cystine-glutamate antiporter System Xc^- (SLC7A11) and inactivation of GPX4, which compromises the cell's capacity to remove phospholipid hydroperoxides *(Autophagy, 2023, 19, 2621-2638)*.
- Lipid peroxidation-iron overload amplification, wherein ACSL4-dependent polyunsaturated fatty acid (PUFA) remodeling, Fenton chemistry, and ferritin degradation (FTH1 loss) create a self-reinforcing loop of oxidative membrane damage *(Autophagy, 2023, 17, 2054-2081)*.

Third, we have expanded our explanation of the dual role of HMOX1, integrating both protective and detrimental mechanisms.

- Under physiological or mildly oxidative conditions, transient HMOX1 induction is cytoprotective through bilirubin/biliverdin production and controlled heme turnover *(Nat Rev Immunol, 2021, 21, 411-425; Mol Neurodegener, 2021, 16, 16).*
- Under pathological oxidative stress, sustained HMOX1 activation promotes the excessive release of Fe^{2+}, which depletes GSH, inhibits GPX4, downregulates

solute carrier family 7 member 11 (SLC7A11)—a key component of the Xc^- system, enhances ACSL4 activity, and fuels Fenton-driven lipid peroxidation. Together, these events create a pro-ferroptotic environment (*Circ Res, 2025, 136, 361-378; Redox Biol, 2014, 2, 273-283*).

These expanded mechanistic explanations have been incorporated into the revised Introduction and Discussion (Lines 53-68; 705-712) to create a more comprehensive and cohesive rationale for the study.

Comment 2: The TEM image of OAMs shows only two micelles in the entire field of view, which is too limited to assess whether the micelles are uniformly distributed. It is recommended to provide images with a larger field of view.

Author's response: Thank you for this valuable suggestion. We have included a larger field-of-view TEM image of OAMs in the Supplementary Information (Supplementary Fig. 2a), clearly demonstrating a uniform, well-dispersed spherical morphology without aggregation.

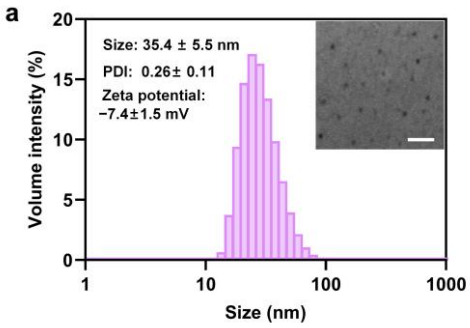

Supplementary Fig. 2a | Hydrodynamic size distribution of OAMs measured by dynamic light scattering (DLS); inset, transmission electron microscopy (TEM) image of micelles. Scale bar, 100 nm.

Comment 3: It is imperative to confirm the chemical structure of OAMs. Techniques such as ^1H NMR spectroscopy and FTIR should be employed to verify that the synthesized polymer is indeed OPDEA and to demonstrate successful drug encapsulation.

Author's response: Thank you for your valuable suggestion. We have incorporated ^{1}H NMR and FTIR characterisation to verify the structure of OPDEA-PCL copolymer and to confirm the successful encapsulation of Art.

The ^{1}H NMR spectrum of OPDEA-PCL shows resonance signals consistent with both polymer blocks (Supplementary Fig. 1): methylene protons from PCL appear at ~4.05 ppm (–O–CH_2–), ~2.30 ppm (–CH_2–C(=O)–), and ~1.65/1.40 ppm (aliphatic –CH_2–); OPDEA side-chain signals protons are observed at ~4.4–4.7 ppm (–O–CH_2–), ~3.3–3.7 ppm (–CH_2– in N-oxide group), and ~1.3–1.4 ppm (–CH_3 in N-oxide group). The integration ratios align well with the targeted block composition.

The FTIR spectrum of OAMs retains the characteristic ester C=O stretching vibration of the polymer (~1720 cm^{-1}) and exhibits absorption bands corresponding to Art (lactone carbonyl: ~1757 cm^{-1}; –OH stretching: ~3240 cm^{-1}) (Supplementary Fig. S2b). Combined with HPLC quantification data and DLS/TEM evidence of uniform micelle formation, these results demonstrate the successful encapsulation of Art.

The corresponding text has been added to the revised manuscript (Lines 128-129; 132-134).

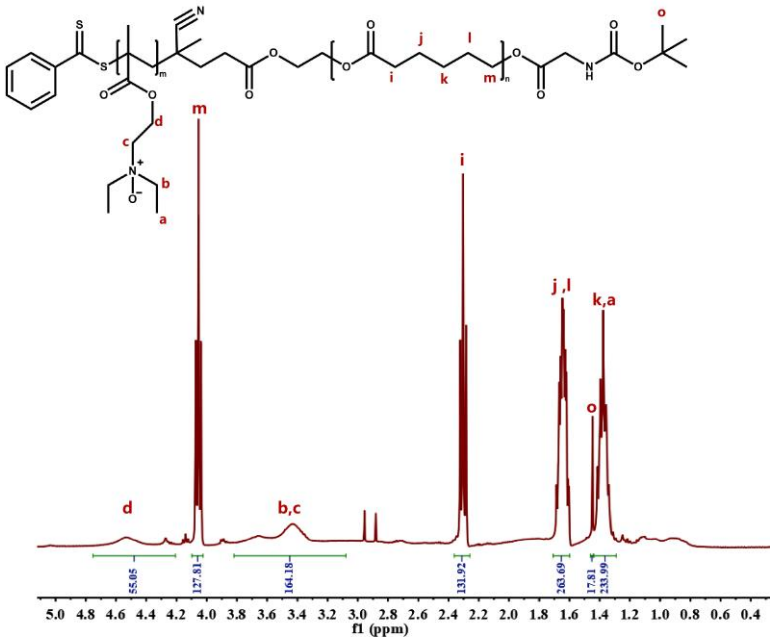

Supplementary Fig. 1 | The ^{1}H NMR spectrum of $OPDEA_{5k}$-PCL_{5k} in $CDCl_3$.

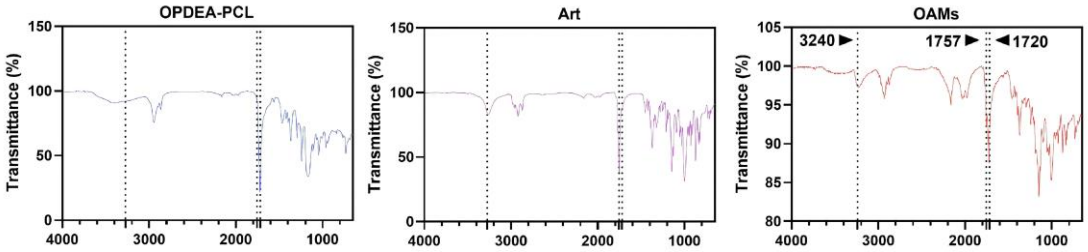

Supplementary Fig. 2b | Fourier-transform infrared (FTIR) spectra of OPDEA–PCL, Art, and OAMs.

Comment 4: A more comprehensive evaluation of the stability of OAMs should be conducted. For example, both the stability and drug release profile of OAMs should be examined under different pH conditions. Moreover, in the paper, the *in vitro* release curve of Art was detected at room temperature. Why not conduct the detection at 37°C?

Author's response: Thank you for these valuable suggestions. To address these points, we have expanded the characterisation by evaluating both colloidal stability and release kinetics under physiologically relevant conditions.

First, the colloidal stability of OAMs was assessed at pH 7.4 (physiological conditions) and pH 6.5 (mimicking peri-ischaemic conditions) by monitoring hydrodynamic diameter and polydispersity index (PDI) over 24 h. The results demonstrate that OAMs exhibit excellent stability at both pH values, with no significant changes in size or PDI (Supplementary Fig. 2d).

Second, we sincerely apologize for the previous lack of clarity. The *in vitro* release studies were conducted at 37 °C, as now clearly specified in the figure captions and Methods section. Moreover, we have incorporated release profiles at pH 6.5 (Supplementary Fig. 2e), revealing a cumulative release of approximately 30% at 24 h, comparable to that observed at pH 7.4.

These updated data have been incorporated into the revised manuscript (Lines 136-140).

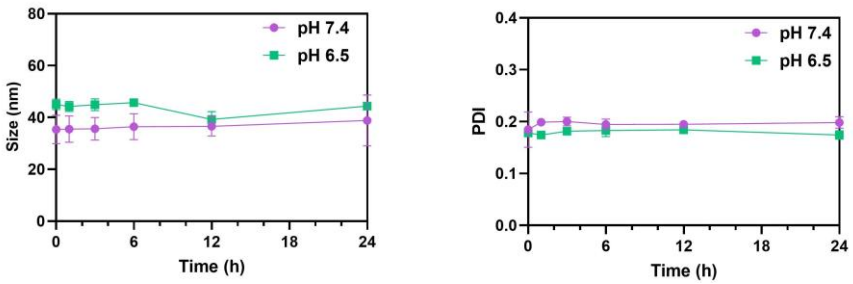

Supplementary Fig. 2d | Evaluation of the colloidal stability of OAMs over time in phosphate-buffered saline (PBS) at 37 ℃ by monitoring the hydrodynamic diameter and polydispersity index (PDI) at pH 7.4 or 6.5.

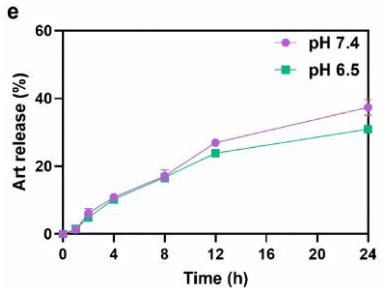

Supplementary Fig. 2e | *In vitro* release profiles of Art from OAMs in PBS (37 °C) at pH 7.4 and pH 6.5 over 24 h (initial Art concentration, 200 μg ml^{-1}).

Comment 5: Does the transport of micelles across the blood-brain barrier and their subsequent accumulation in the brain are affected by I/R injury? Are there differences observed between healthy mice and those subjected to CA/CPR models?

Author's response: Thank you for raising this insightful question. To address whether I/R injury influences BBB transport of our nanocarrier, we performed a direct comparative analysis of OPDEA-^{Cy5}PCL micelle accumulation in healthy versus CA/CPR mice using *ex vivo* fluorescence imaging.

Our results show that OPDEA-^{Cy5}PCL micelles showed moderately higher brain fluorescence at 3 and 12 h post-injection in CA/CPR mice, with levels converging with Sham animals by 24 h (Supplementary Fig. 3l,m). This temporal profile matches the characteristic biphasic BBB response to global I/R injury, in which early oxidative and inflammatory stress leads to loosening of tight junctions, thereby increasing paracellular permeability, followed by gradual barrier restoration. Importantly, even

under healthy physiological conditions, where the BBB remains intact, OPDEA-PCL micelles still achieve robust brain delivery. These findings suggest that OPDEA-PCL micelles predominantly cross the BBB *via* AMT. The transient BBB compromise in CA/CPR animals likely provides an auxiliary entry route, enhancing early accumulation without altering the underlying AMT-based delivery capability of the OPDEA platform.

All experimental details and the corresponding data have been added to the revised manuscript (Lines 198-209).

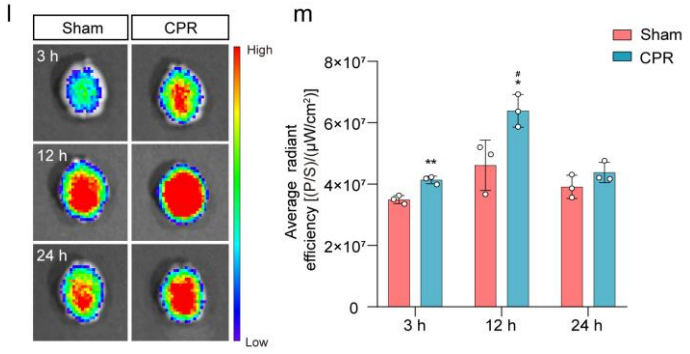

Supplementary Fig. 3l,m | *Ex vivo* fluorescence imaging (**l**) and quantification (**m**) of brain tissues from Sham and CPR mice at 3, 12, and 24 h post-injection of OPDEA–^{Cy5}PCL micelles (n = 3 mice). Cy5-equivalent dose, 100 μg kg^{-1}. Data are presented as mean ± SD. Statistical significance was determined by a two-tailed unpaired Student's t test (two groups) or one-way ANOVA with Tukey's post hoc test (multiple groups). *P < 0.05, **P < 0.01 vs. Sham group; $^{\#}P$ < 0.05 vs. CPR (24 h) group.

Comment 6: Immunofluorescence staining of frozen sections using markers for endothelial cells (CD31), neurons (NeuN), and microglia (Iba1) did not reveal robust colocalization of OPDEA-^{Cy5}PCL fluorescence with these three cell types. While these results indicate that the micelles can cross the BBB and reach brain tissue, they do not demonstrate specific accumulation within the aforementioned cell populations.

Author's response: Thank you for your thoughtful comment. We agree that our original wording could be misinterpreted as implying cell-type-specific targeting, which was not our intention. We aimed to show that OPDEA-^{Cy5}PCL micelles reach the

brain parenchyma and become associated with multiple cell types within the neurovascular unit, rather than to demonstrate selective accumulation in any single population.

To clarify, in the revised text, we now explicitly describe what was quantified: using ImageJ, we segmented $CD31^+$ endothelial cells, $NeuN^+$ neurons, and $Iba1^+$ microglia, and measured the mean Cy5 intensity within cells. Compared with the PEG micelle and free-dye controls, all three cell populations exhibited a significant increase in OPDEA-^{Cy5}PCL-derived Cy5 signal, indicating that the micelles can traverse the BBB and enter the brain parenchyma, where they are taken up or retained by endothelial cells, neurons, and microglia. However, the Cy5 signal was not tightly confined to any single marker-defined population, and we therefore do not claim specific targeting or robust co-localisation with a particular cell type.

The relevant sentence in the manuscript has been revised to read:

"Notably, compared with minimal fluorescence in the control groups, OPDEA-^{Cy5}PCL micelles produced substantial intracellular Cy5 signals in all three cell populations (Fig. 2e–g; Supplementary Fig. 3i–k), confirming that OPDEA-PCL micelles can cross the BBB, distribute within the brain parenchyma, and finally enter endothelial, neuronal, and microglial compartments."

These clarifications have been included in the revised manuscript (Lines 188-192).

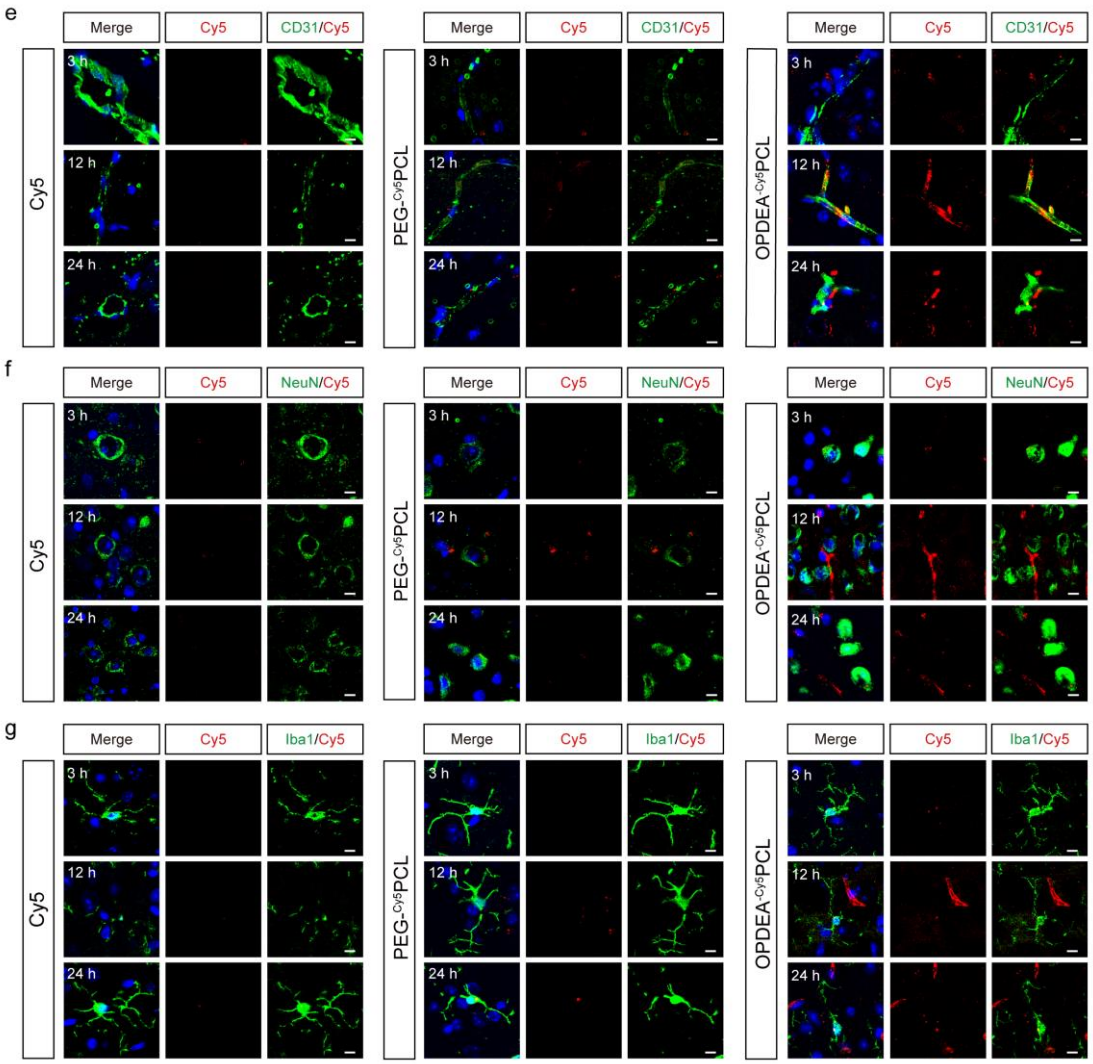

Fig. 2e-g | Immunofluorescence images of brain cryosections showing the distribution of PEG-^{Cy5}PCL or OPDEA-^{Cy5}PCL micelles (red) and free Cy5 within CD31^{+} endothelial cells (**e**), NeuN^{+} neurons (**f**), and Iba1^{+} microglia (**g**). Cell-type markers (CD31, NeuN, Iba1) were detected using Alexa Fluor 488-conjugated antibodies (green), and nuclei were stained with DAPI (blue). n = 3 mice. Cy5-equivalent dose, 100 μg kg^{-1}. Scale bar, 10 μm.

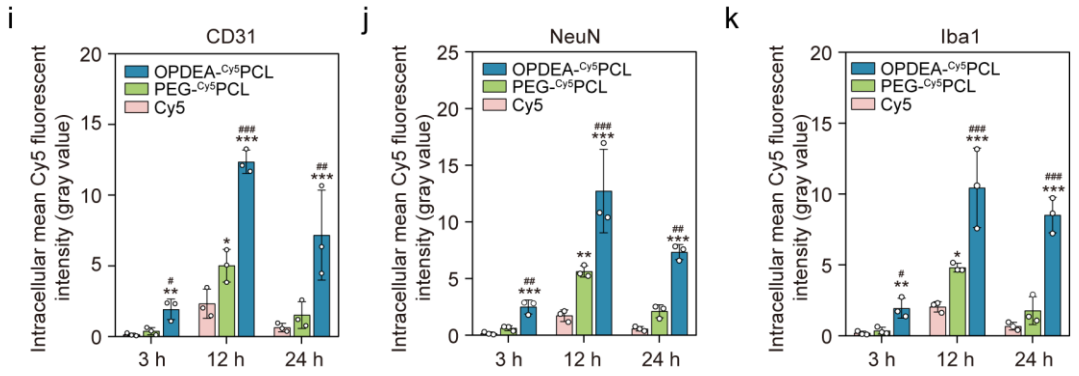

Supplementary Fig. 3i-k | Quantification of Cy5 fluorescence in $CD31^+$ endothelial cells (**i**), $NeuN^+$ neurons (**j**), and $Iba1^+$ microglia (**k**) at designated time points after *i.v.* administration of free Cy5, PEG–^{Cy5}PCL, or OPDEA–^{Cy5}PCL micelles (n = 3 mice; 3 randomly selected fields per sample). Cy5-equivalent dose, 100 μg kg^{-1}. Data are presented as mean ± SD. Statistical significance was determined by one-way ANOVA with Tukey's post hoc test (multiple groups). $^{*}P < 0.05$, $^{***}P < 0.001$ vs. Cy5 group; $^{\#\#}P < 0.01$, $^{\#\#\#}P < 0.001$ vs. PEG-^{Cy5}PCL group.

Comment 7: The text states that these micelles accumulate in the neurovascular unit and inflammatory cells; however, subsequent cellular experiments only examined endothelial cells and neurons. Why was the internalization of these micelles not investigated in microglia? It is recommended to supplement these experiments.

Author's response: Thank you for your valuable suggestion. In line with your recommendation, we have now explicitly investigated microglial internalisation of the micelles using BV2 cells. Confocal microscopy and flow cytometry quantification demonstrated that OPDEA-^{Cy5}PCL micelles exhibited significantly higher uptake than PEG-^{Cy5}PCL at 24 h (Supplementary Fig. 4a, f-g), consistent with the enhanced cell-membrane engagement conferred by the OPDEA corona. As BV2 microglia possess intrinsic phagocytic activity, they also internalised PEGylated micelles to a greater extent than non-phagocytic endothelial and neuronal cells, which explains the relatively elevated Cy5 signal in the PEG control group. We further characterised exocytosis kinetics in BV2 cells and observed that BV2 cells displayed a cumulative exocytosis

rate of ~64.0% by 12 h (Supplementary Fig. 4k, l). These findings complement our neurovascular unit analyses and confirm that OPDEA-PCL micelles are effectively transcytosed by microglia following BBB translocation.

The corresponding data have been incorporated into the revised manuscript (Lines 215-218; 278-280).

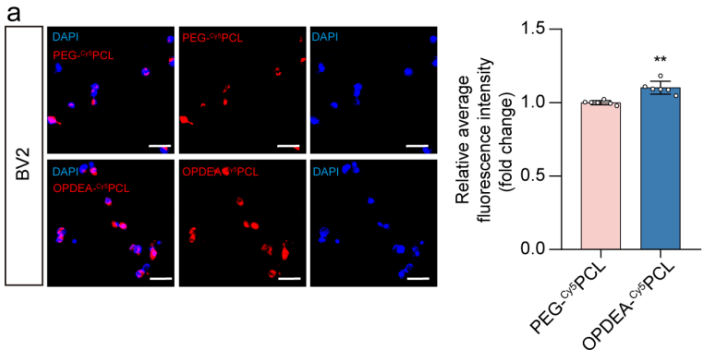

Supplementary Fig. 4a | Confocal microscopy images (left) and quantitative analysis (right) of cellular uptake of Cy5-labelled OPDEA–PCL micelles by BV2 microglial cells after 24 h incubation (n = 6 biological replicates). Nuclei were stained with DAPI (blue). Cy5-equivalent dose, 0.5 μg ml^{-1}. Scale bar, 20 μm. Data are presented as mean ± SD. Statistical significance was determined by two-tailed unpaired Student's t test. $^{**}P < 0.01$.

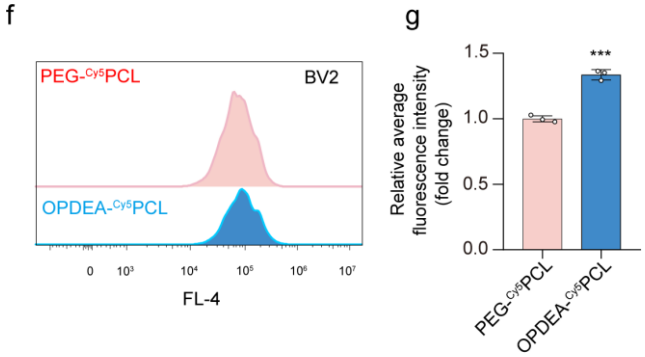

Supplementary Fig. 4f,g | Representative flow cytometry histograms (**f**) and corresponding quantification (**g**) of Cy5-labelled micelle uptake in BV2 microglial cells after 24 h incubation (n = 3). Cy5-equivalent dose, 0.5 μg ml^{-1}. Data are presented as mean ± SD. Statistical significance was determined by two-tailed unpaired Student's t

test. ***$P < 0.001$.

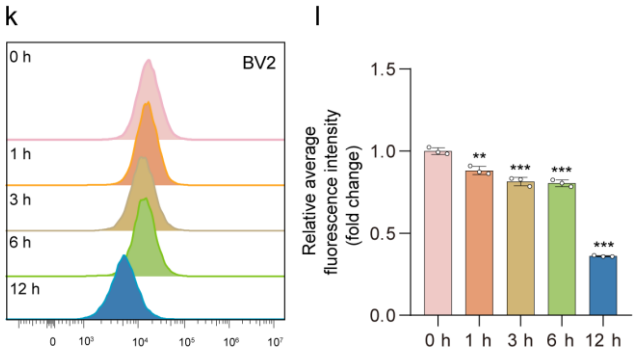

Supplementary Fig. 4k,l | Representative flow cytometry histogram (**k**) and quantification (**l**) of time-dependent exocytosis of OPDEA–^{Cy5}PCL micelles from BV2 microglial cells. Cells were pre-incubated with micelles for 24 h, washed, and transferred to fresh medium for the indicated durations (n = 3 biological replicates). Cy5-equivalent dose, 0.5 μg ml^{-1}. Data are presented as mean ± SD. Statistical significance was determined by one-way ANOVA with Dunnett's multiple comparison test (multiple groups). **$P < 0.01$, ***$P < 0.001$.

Comment 8: Experimental results demonstrate that the micelles within neuronal cells undergo rapid and efficient efflux (50.1% efflux at 3 hours, 60% at 6 hours). If the drug cannot accumulate effectively in neuronal cells, how can it exert subsequent therapeutic effects?

Author's response: Thank you for your insightful comment. We agree that interpreting the efflux data at the single-cell level requires careful consideration of the overall delivery mechanism. In our system, the therapeutic efficacy of OAMs does not depend solely on long-term retention of micelles within individual neurons, but rather on their capacity to (i) repeatedly undergo AMT and (ii) achieve broad tissue-level distribution and sustained drug exposure in the brain.

First, the ~50-60% efflux observed at 3-6 h in HT22 cells reflects micellar carrier dynamics, rather than the complete loss of the drug from the tissue. During their intracellular residence, OAMs can release a fraction of Art, enabling local drug action even as some micelles are exocytosed. Second, the exocytosed micelles are not simply

“lost”; they can be taken up by neighbouring cells (endothelial cells, neurons, and microglia), effectively facilitating an intercellular relay of the nanocarrier and promoting more homogeneous drug distribution across the hippocampal microenvironment. This is consistent with our *in vivo* data, which show efficient BBB traversal, widespread brain accumulation, and intense Cy5 signal in multiple cell populations (Fig. 2c-g). Most importantly, the functional outcomes—reduced ferroptotic markers, preserved mitochondrial function, attenuated neuronal loss, and improved neurological scores in CA/CPR mice—demonstrate that, despite partial efflux at the single-cell level, the overall tissue-level exposure achieved by OAMs is sufficient to exert robust and durable neuroprotection.

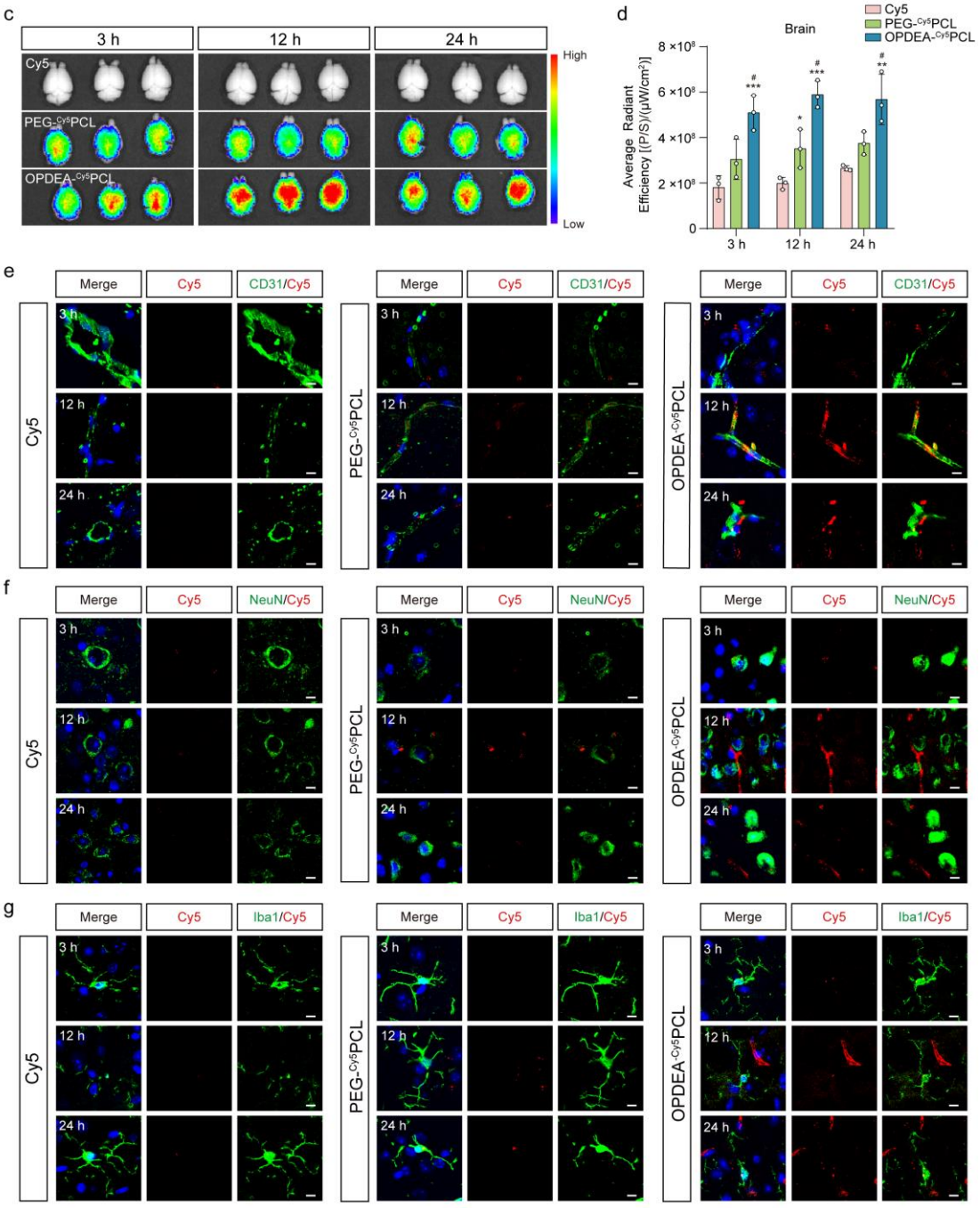

Fig. 2 c-g | c, d, *Ex vivo* near-infrared fluorescence imaging (**c**) and quantitative analysis (**d**) of Cy5 fluorescence in whole-brain tissues collected at the indicated time points after *i.v.* administration of free Cy5, PEG-^{Cy5}PCL, or OPDEA-^{Cy5}PCL micelles in mice (n = 3). Cy5-equivalent dose, 100 μg kg^{-1}. **e–g**, Immunofluorescence images of brain cryosections showing the distribution of PEG-^{Cy5}PCL or OPDEA-^{Cy5}PCL micelles (red) and free Cy5 within CD31^{+} endothelial cells (**e**), NeuN^{+} neurons (**f**), and Iba1^{+} microglia (**g**). Cell-type markers (CD31, NeuN, Iba1) were detected using Alexa Fluor

488-conjugated antibodies (green), and nuclei were stained with DAPI (blue). $n = 3$ mice. Cy5-equivalent dose, 100 μg kg^{-1}. Scale bar, 10 μm. Data are presented as mean ± SD. Statistical significance was determined by one-way ANOVA with Tukey's post hoc test (multiple groups). $^{*}P < 0.05$, $^{**}P < 0.01$, $^{***}P < 0.001$ vs. Cy5; $^{\#}P < 0.05$ vs. PEG-^{Cy5}PCL.

Comment 9: Neuroinflammation is primarily triggered by the activation of glial cells (microglia), and TNF-α and IL-1β are also predominantly produced by microglia. Therefore, merely detecting the expression of TNF-α and IL-1β in HT22 cells *via* qPCR does not sufficiently demonstrate that OAMs alleviate inflammatory signaling under H/R challenge.

Author's response: Thank you for raising this important point. We fully agree that microglia are the principal cellular drivers of neuroinflammation after I/R injury and that TNF-α and IL-1β are predominantly produced by activated microglia rather than neurons alone. To address this, we performed *in vitro* H/R assays in BV2 microglial cells to evaluate the anti-inflammatory effects of OAMs. Our results show that OAM treatment significantly reduced *Tnf* and *Il1b* mRNA expression and decreased the secretion of TNF-α and IL-1β proteins compared with control groups (Supplementary Fig. 6a-d), indicating a direct suppression of microglial pro-inflammatory output. To further characterise microglial phenotype, we performed immunofluorescence staining for iNOS (M1/pro-inflammatory marker) and Arg1 (M2/reparative marker). H/R stimulation drove BV2 cells toward an M1-like state, as evidenced by robust upregulation of iNOS. In contrast, OAM treatment significantly decreased iNOS and increased Arg1 fluorescence intensity (Supplementary Fig. 6e-h), suggesting a shift from a pro-inflammatory M1 phenotype toward a reparative M2 phenotype (*Adv. Sci., 2025, 12, e2408992*).

These findings demonstrate that OAMs alleviate H/R-induced inflammatory signalling not only at the neuronal level but also by modulating microglial activation and polarisation, which are crucial to the neuroinflammatory cascade. The corresponding methods and descriptions have been incorporated into the revised

manuscript (Lines 345-358).

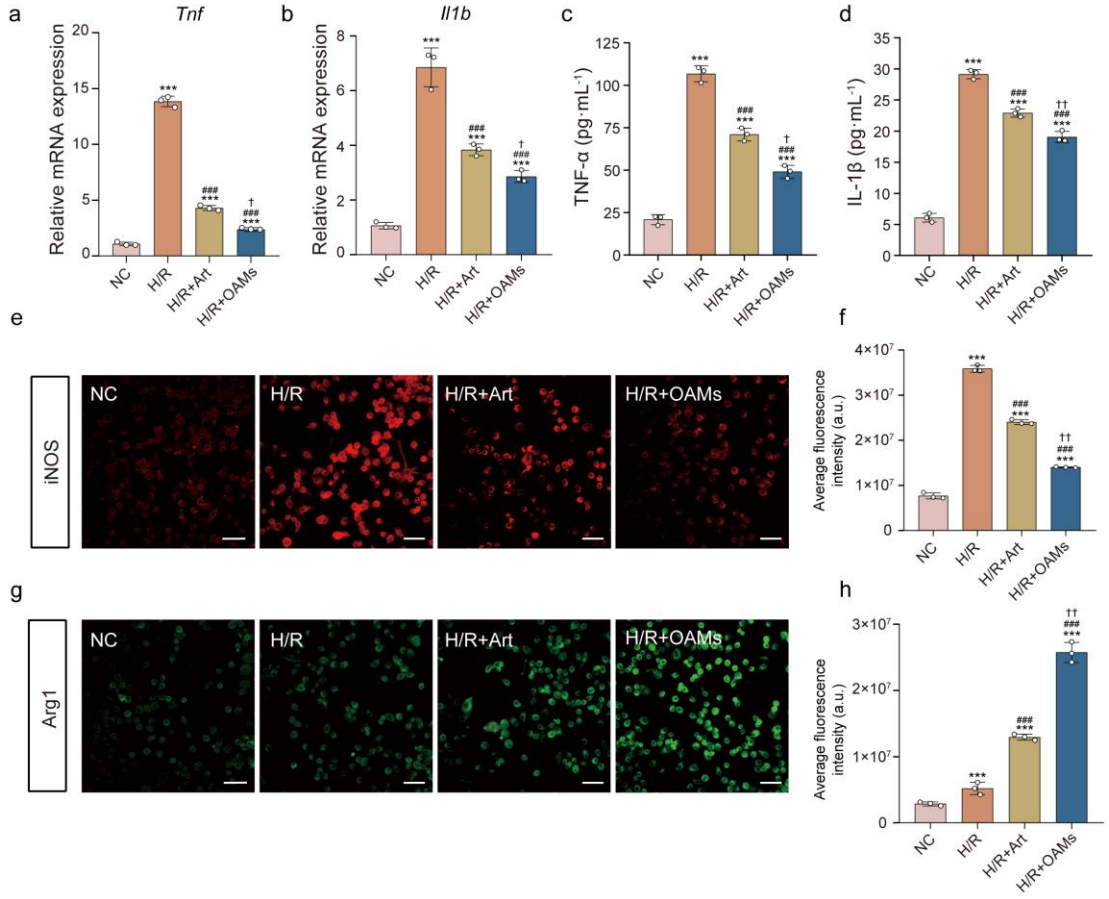

Supplementary Fig. 6 | OAMs attenuate microglial inflammation and reprogramme microglial polarisation. a–d, Relative mRNA expression of *Tnf* (**a**) and *Il1b* (**b**) in BV2 microglial cells treated with OAMs for 24 h under hypoxia–reoxygenation (H/R), as assessed by qRT–PCR; corresponding TNF-α (**c**) and IL-1β (**d**) protein levels in culture supernatants measured by ELISA (n = 3 biological replicates). Art-equivalent dose, 250 nM. **e–h**, Immunofluorescence images of BV2 cells stained for the M1 marker iNOS (red) and M2 marker Arg1 (green) after 24 h of H/R with or without OAMs (**e, g**), and quantification of iNOS (**f**) and Arg1 (**h**) fluorescence intensity (n = 3 biological replicates). Art-equivalent dose, 250 nM. Scale bar, 100 μm. Data are presented as mean ± SD. Statistical significance was determined by one-way ANOVA with Tukey's post hoc test (multiple groups). ***$P < 0.001$ vs. NC; $^{\#}P < 0.05$, $^{\#\#}P < 0.01$, $^{\#\#\#}P < 0.001$ vs. H/R; $^{\dagger}P < 0.05$, $^{\dagger\dagger}P < 0.01$ vs. H/R+Art.

Comment 10: The results of TUNEL staining and immunohistochemical staining for cleaved-caspase-3 are weak and fail to convincingly demonstrate the anti-apoptotic effects of OAMs. It is recommended to supplement these findings with Western blot experiments targeting key molecules involved in classical apoptotic pathways.

Author's response: Thank you for this valuable suggestion. In response, we have supplemented protein-level analyses of key regulators in the intrinsic apoptotic pathway in hippocampal tissues from CA/CPR mice, with or without OAM treatment.

Specifically, we performed Western blotting for Bcl-2, BAX, and cleaved caspase-3. Bcl-2 and BAX are central mitochondrial gatekeepers that regulate cytochrome c release, while cleaved caspase-3 is a terminal executioner of apoptosis. CA/CPR markedly decreased Bcl-2 expression and increased BAX and cleaved caspase-3 levels compared with sham controls. Importantly, OAM administration significantly upregulated Bcl-2 and concomitantly downregulated BAX and cleaved caspase-3 relative to both CA/CPR and Art groups (Supplementary Fig.11), indicating suppression of mitochondrial apoptotic signalling.

The corresponding results and descriptions have been incorporated into the revised manuscript (Lines 394-395).

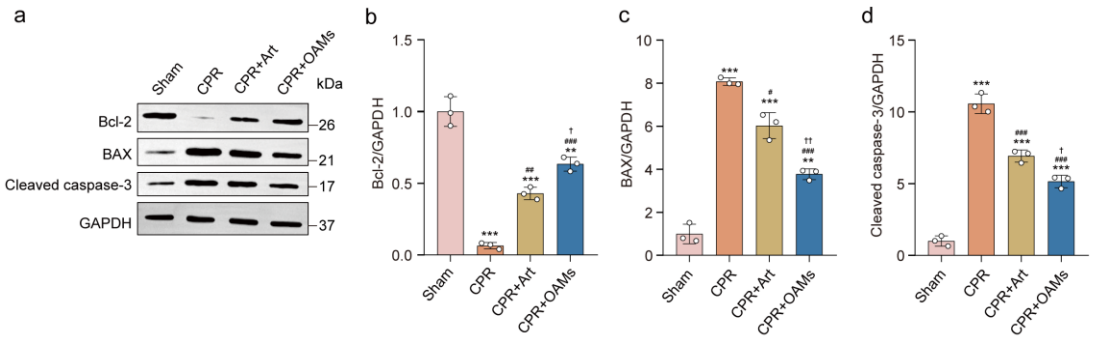

Supplementary Fig. 11 | OAM-mediated regulation of apoptotic pathways after CA/CPR. Representative western blots (**a**) and quantification of hippocampal expression of Bcl-2 (**b**), BAX (**c**), and cleaved caspase-3 (**d**) at 24 h after ROSC in mice receiving *i.v.* administration of the indicated treatments immediately post-ROSC ($n = 3$ mice). Art-equivalent dose, 5 mg kg^{-1}. Data are presented as mean ± SD. Statistical significance was determined by one-way ANOVA with Tukey's post hoc test (multiple

groups). $^{**}P < 0.01$, $^{***}P < 0.001$ vs. Sham; $^{\#}P < 0.05$, $^{\#\#}P < 0.01$, $^{\#\#\#}P < 0.001$ vs. CPR; $^{\dagger}P < 0.05$, $^{\dagger\dagger}P < 0.01$ vs. CPR+Art.

Comment 11: The article relies solely on measuring intracellular iron levels, lipid peroxidation, and GSH levels to establish the relationship between HMOX1 activity and the execution of ferroptosis in neurons, which is insufficiently comprehensive. It is necessary to supplement these data with WB analyses of key molecules involved in the classical ferroptosis pathway.

Author's response: Thank you for your insightful suggestion. In line with your recommendation, we have strengthened the mechanistic evidence by adding Western blot analyses of key regulators in the canonical ferroptosis pathway, including GPX4 (lipid hydroperoxide detoxification), ACSL4 (PUFA-phospholipid enrichment), and FTH1 (iron sequestration).

First, in HT22 neurons subjected to H/R, HMOX1 overexpression led to a ferroptosis-favouring protein profile, characterised by reduced FTH1 and GPX4 expression and increased ACSL4 expression (Supplementary Fig. 14c-f), consistent with expansion of the labile iron pool and enhanced lipid peroxidation. Second, HMOX1 knockdown reversed these changes under both H/R and RSL3 challenge, restoring FTH1 and GPX4 expression while suppressing ACSL4 expression (Supplementary Fig. 15n-q and 16i-l), indicating that HMOX1 is an upstream regulator of these ferroptosis effectors. Third, OAM treatment promoted the recovery of FTH1 and GPX4 expression and attenuated ACSL4 upregulation in the *in vitro* H/R model (Supplementary Fig. 17c-f) and in hippocampal tissue after CA/CPR *in vivo* (Supplementary Fig. 18a-d), linking its neuroprotective effect to correction of ferroptotic signalling.

These protein-level data align with our measurements of intracellular iron, lipid peroxidation, and GSH levels, and support a coherent mechanistic cascade: H/R-induced HMOX1 activation expands the labile iron pool and shifts the GPX4-ACSL4-FTH1 axis toward ferroptosis, whereas OAMs inhibit HMOX1, enhance iron storage, preserve antioxidant defence, and dampen ACSL4-driven lipid peroxidation.

The corresponding results and methodological details have been incorporated into the revised manuscript (Lines 500-509; 516; 519-525; 617-619; 663-666).

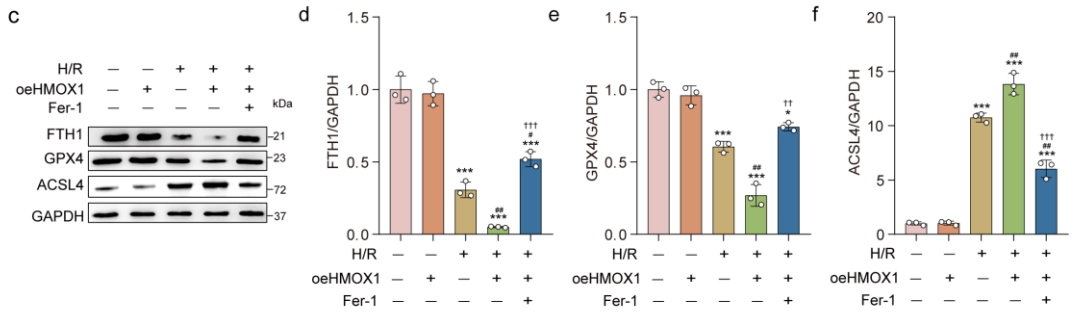

Supplementary Fig. 14c-f | Representative western blots (**c**) and quantitative analysis of ferroptosis-related proteins FTH1 (**d**), GPX4 (**e**), and ACSL4 (**f**), with GAPDH as loading control. Fer-1 dose, 5 μM. n = 3 biological replicates. Data are presented as mean ± SD. Statistical significance was determined by one-way ANOVA with Tukey's post hoc test (multiple groups). $^{*}P < 0.05$, $^{***}P < 0.001$ vs. NC; $^{\#}P < 0.05$, $^{\#\#}P < 0.01$ vs. H/R; $^{\dagger\dagger}P < 0.01$, $^{\dagger\dagger\dagger}P < 0.001$ vs. H/R+oeHMOX1.

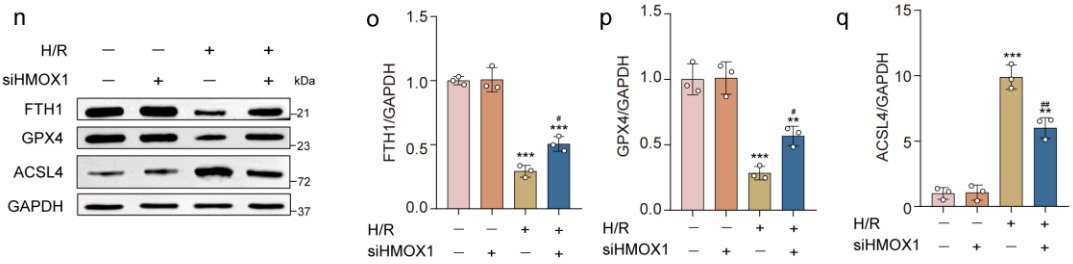

Supplementary Fig. 15n-q | Representative western blots (**n**) and relative expression of FTH1 (**o**), GPX4 (**p**), and ACSL4 (**q**) in siNC and siHMOX1 cells under H/R for 24 h, with GAPDH as loading control. n = 3 biological replicates. Data are presented as mean ± SD. Statistical significance was determined by one-way ANOVA with Tukey's post hoc test (multiple groups). $^{**}P < 0.01$, $^{***}P < 0.001$ vs. NC; $^{\#}P < 0.05$, $^{\#\#}P < 0.01$ vs. H/R.

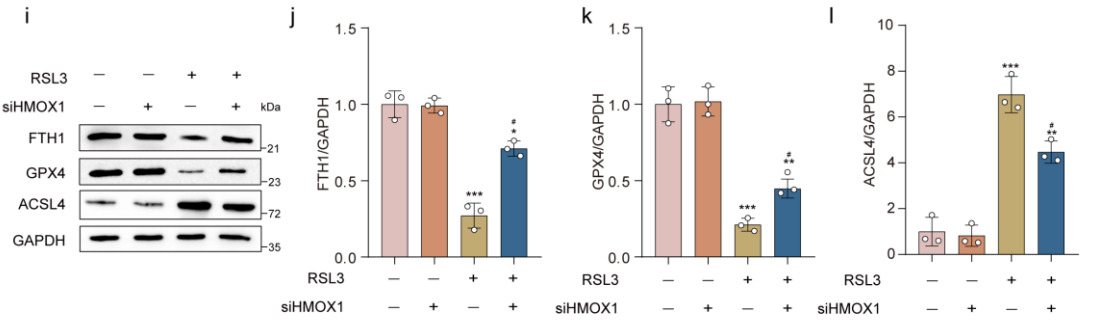

Supplementary Fig. 16i-l | Representative western blots (**i**) and relative expression of FTH1 (**j**), GPX4 (**k**), and ACSL4 (**l**) in siNC and siHMOX1 cells treated with RSL3 for 24 h, with GAPDH as loading control. RSL3 dose, 150 nM. $n = 3$ biological replicates. Data are presented as mean ± SD. Statistical significance was determined by one-way ANOVA with Tukey's post hoc test (multiple groups). $^{*}P < 0.05$, $^{**}P < 0.01$, $^{***}P < 0.001$ vs. NC; $^{\#}P < 0.05$ vs. RSL3.

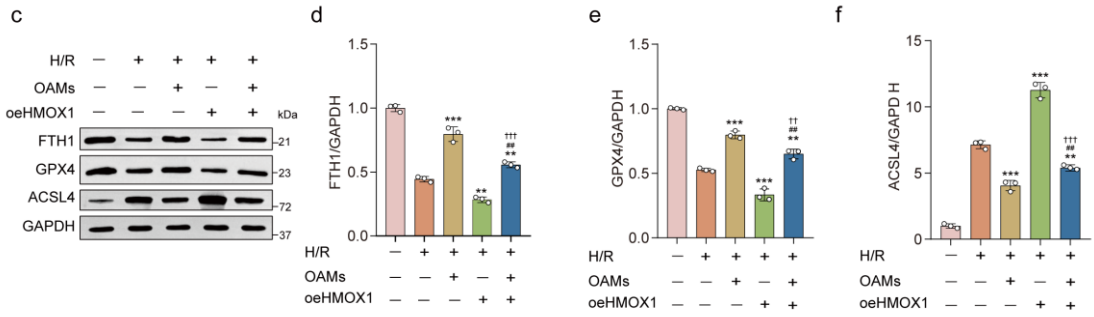

Supplementary Fig. 17c-f | Representative western blots (**c**) and relative expression levels of FTH1 (**d**), GPX4 (**e**), and ACSL4 (**f**) in control and oeHMOX1 HT22 cells treated with OAMs under H/R conditions for 24 h. Art-equivalent dose, 250 nM. $n = 3$ biological replicates. Data are presented as mean ± SD. Statistical significance was determined by one-way ANOVA with Tukey's post hoc test (multiple groups). $^{**}P < 0.01$, $^{***}P < 0.001$ vs. H/R; $^{\#\#}P < 0.01$ vs. H/R+OAMs; $^{\dagger\dagger}P < 0.01$, $^{\dagger\dagger\dagger}P < 0.001$ vs. H/R+oeHMOX1.

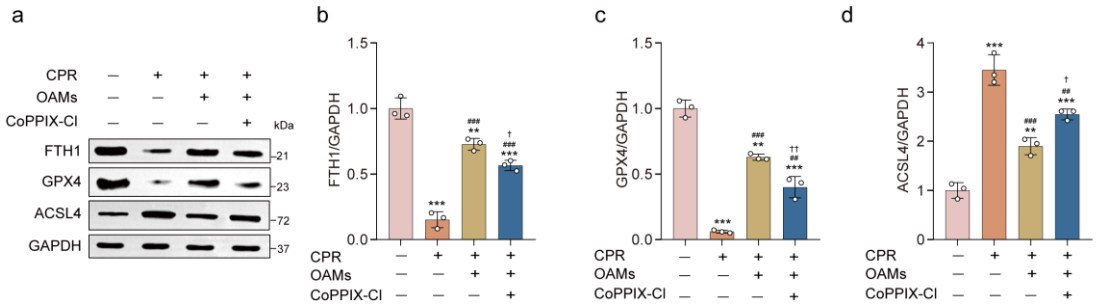

Supplementary Fig. 18 | CoPPIX-Cl–mediated HMOX1 activation weakens OAM-mediated regulation of ferroptosis-related proteins in CA/CPR mice. For CA/CPR mice receiving OAMs, CoPPIX-Cl, or their combination immediately after ROSC, representative western blot bands (**a**) and relative expression of FTH1 (**b**), GPX4 (**c**), and ACSL4 (**d**) in hippocampal tissue at 24 h post-ROSC (n = 3 mice). Art-equivalent dose, 5 mg kg^{-1}; CoPPIX-Cl–equivalent dose, 10 mg kg^{-1}. Data are presented as mean ± SD. Statistical significance was determined by one-way ANOVA with Tukey's post hoc test (multiple groups). $^{**}P < 0.01$, $^{***}P < 0.001$ vs. Sham; $^{\#\#}P < 0.01$, $^{\#\#\#}P < 0.001$ vs. CPR; $^{\dagger}P < 0.05$, $^{\dagger\dagger}P < 0.01$ vs. CPR+OAMs.

Comment 12: Why does overexpression of HMOX1 under normal conditions not activate ferroptosis, whereas under H/R conditions it exacerbates ferroptosis? It is recommended to supplement with further experiments to investigate the specific mechanism by which HMOX1 activates ferroptosis.

Author's response: Thank you for your insightful suggestion. We agree that the pro-ferroptotic role of HMOX1 is context-dependent and emerges predominantly under conditions of oxidative and metabolic stress, when iron-buffering capacity and antioxidant defences are compromised.

Under physiological conditions, basal HMOX1 activity supports haem turnover, while the labile iron pool is tightly regulated by ferritin (FTH1)-mediated sequestration, ferroportin-dependent export, and an intact GSH-GPX4 axis. In this setting, HMOX1 overexpression alone does not expand the labile iron pool beyond the threshold required to initiate ferroptosis. By contrast, H/R stress depletes GSH, disrupts mitochondrial redox homeostasis, and promotes phospholipid radical formation, thereby lowering the

threshold for Fe^{2+}-driven lipid peroxidation and unmasking the pro-ferroptotic potential of HMOX1 (*Redox Biol., 2024, 76, 103345*).

Guided by this rationale and prior work (*Cell Commun. Signal., 2024, 22, 376; Biochem. Pharmacol., 2024, 226, 116346*), we investigated nuclear receptor coactivator 4 (NCOA4)-mediated ferritinophagy as a mechanistic bridge between HMOX1 activation and ferroptosis under H/R. H/R stress induced robust HMOX1 upregulation and excessive haem degradation, leading to an increased the labile iron pool (Fig. 7c). In HT22 neurons subjected to H/R, HMOX1 overexpression further elevated NCOA4 expression, reduced FTH1 levels, and increased the LC3-II/LC3-I ratio (Fig. 8a-d), consistent with activation of NCOA4-driven ferritinophagy. Co-immunoprecipitation further confirmed enhanced NCOA4-FTH1 interaction (Fig. 8e), indicating accelerated ferritin degradation.

To determine whether NCOA4-mediated ferritinophagy is required for HMOX1-driven ferroptosis, we silenced NCOA4 in HMOX1-overexpressing neurons under H/R conditions (Fig. 8f,g). NCOA4 knockdown significantly rescued cell viability (Fig. 8h), reduced cytosolic Fe^{2+} accumulation (Fig. 8i) and lipid peroxidation (Fig. 8j), restored GSH levels (Fig. 8k), and attenuated lipid ROS (Fig. 8l,m). At the protein level, this intervention normalised key ferroptosis regulators, with NCOA4 and ACSL4 downregulated, whereas FTH1 and GPX4 upregulated (Fig. 8n-r).

Taken together, these results support a stress-gated cascade in which H/R-induced HMOX1 activation expands the labile iron pool, triggers NCOA4-dependent ferritinophagy, further aggravates iron overload, and amplifies ferroptosis. Under basal conditions, intact iron-buffering systems prevent engagement of this loop, explaining why HMOX1 overexpression alone is insufficient to initiate ferroptosis. These mechanistic insights and the supporting experimental data have been incorporated into the revised manuscript (Lines 587-598; 723-730).

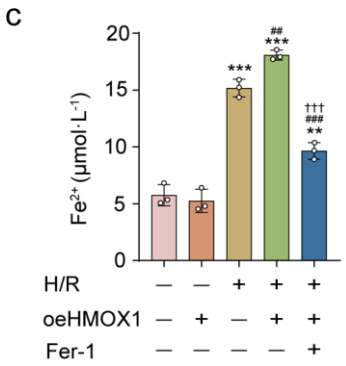

Fig. 7c | Intracellular Fe^{2+} levels determined by the ferrozine colourimetric assay. Fer-1 dose, 5 μM. $n = 3$ biological replicates. Data are presented as mean ± SD. Statistical significance was determined by one-way ANOVA with Tukey's post hoc test (multiple groups). $^{**}P < 0.01$, $^{***}P < 0.001$ vs. NC+oeHMOX1; $^{\#\#}P < 0.01$, $^{\#\#\#}P < 0.001$ vs. H/R; $^{\dagger\dagger\dagger}P < 0.001$ vs. H/R+oeHMOX1.

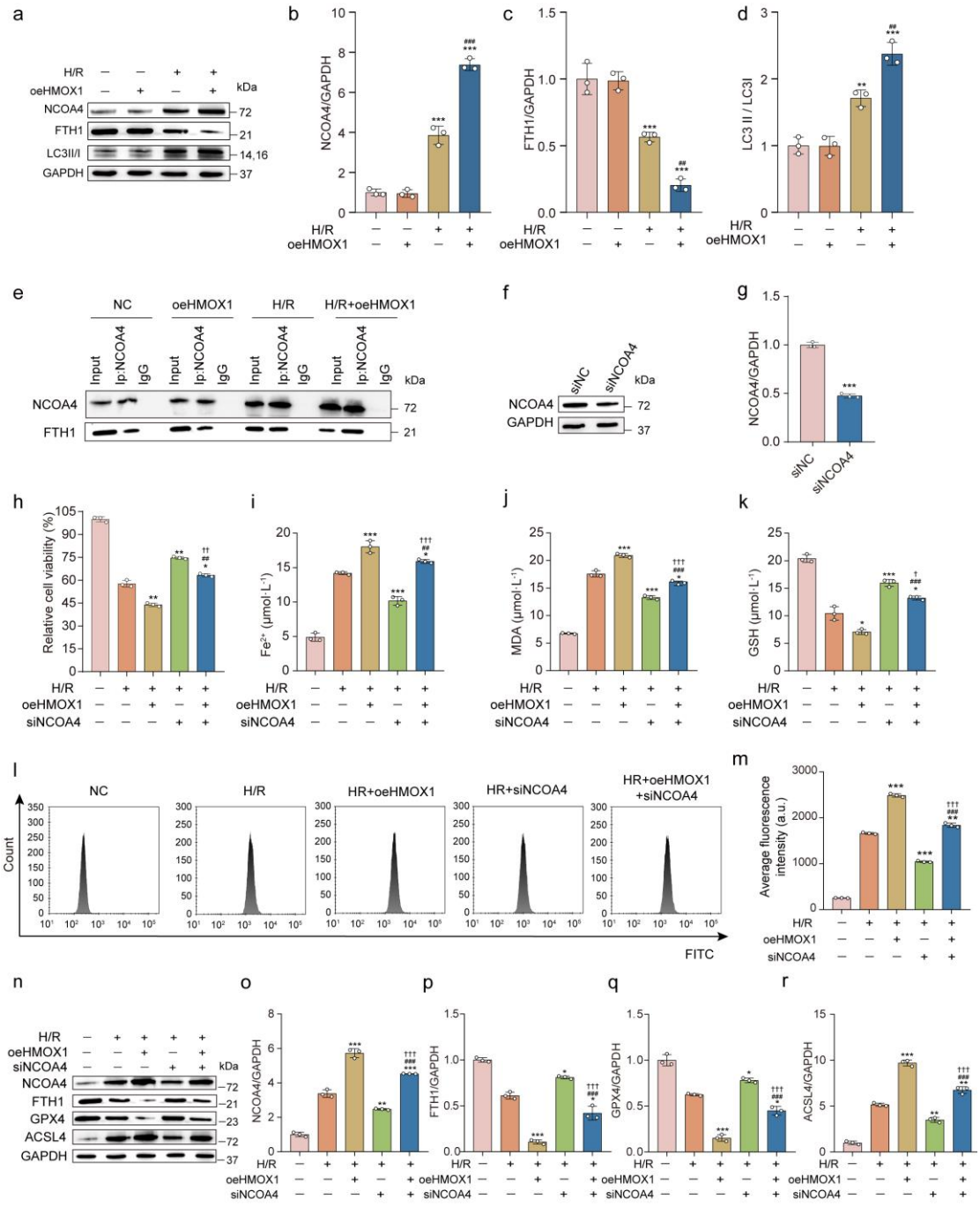

Fig. 8 | Excessive HMOX1 activation exacerbates ferroptosis *via* NCOA4-mediated ferritinophagy following H/R injury. a–d, Representative western blots (**a**) and quantification of NCOA4 (**b**), FTH1 (**c**), and LC3-II/I ratios (**d**) in normal and oeHMOX1 HT22 cells subjected to H/R for 24 h. **e**, Co-IP analysis of NCOA4–FTH1 interaction in normal and oeHMOX1 HT22 cells under H/R conditions. **f, g**, Representative western blots (**f**) and quantification (**g**) validating NCOA4 knockdown efficiency in HT22 cells transfected with siNCOA4 or siNC under normoxic conditions.

h, Cell viability of HT22 cells after indicated treatments measured by CCK-8 assay. **i–k**, Cytosolic Fe^{2+} levels (**i**), MDA content (**j**), and GSH levels (**k**) in HT22 cells. **l, m**, Representative flow cytometry histograms (**l**) and quantification (**m**) of cytosolic lipid ROS in HT22 cells detected using the C11-BODIPY 581/591 probe. **n–r**, Representative western blots (**n**) and quantification of NCOA4 (**o**), FTH1 (**p**), GPX4 (**q**), and ACSL4 (**r**) in HT22 cells. $n = 3$ biological replicates. Data are presented as mean ± SD. Statistical significance was determined by a two-tailed unpaired Student's *t* test (two groups) or one-way ANOVA with Tukey's post hoc test (multiple groups). In panel a–g: $^{**}P < 0.01$, $^{***}P < 0.001$ vs. NC; $^{\#\#}P < 0.01$, $^{\#\#\#}P < 0.001$ vs. H/R. In panel h–r: $^{*}P < 0.05$, $^{**}P < 0.01$, $^{***}P < 0.001$ vs. H/R; $^{\#}P < 0.05$, $^{\#\#}P < 0.01$, $^{\#\#\#}P < 0.001$ vs. H/R+oeHMOX1; $^{\dagger}P < 0.05$, $^{\dagger\dagger}P < 0.01$, $^{\dagger\dagger\dagger}P < 0.001$ vs. H/R+siNCOA4.

Comment 13: The production of mitochondrial reactive oxygen species is closely related to the mitochondrial membrane potential. Therefore, it is recommended to supplement the study with detection results of mitochondrial membrane potential under different conditions (e.g., JC-1 staining).

Author's response: Thank you for your valuable suggestion. In line with your recommendation, we have assessed mitochondrial membrane potential (ΔΨm) using JC-1 staining in HT22 neurons under different experimental conditions. In this assay, intact, highly polarised mitochondria promote JC-1 aggregation in the matrix, yielding red fluorescence, whereas mitochondrial depolarisation leads to dissociation into green-fluorescent monomers. The red-to-green fluorescence ratio, quantified by flow cytometry, was used as an index of ΔΨm integrity.

Our data clearly demonstrate that H/R stress led to a significant loss of ΔΨm. This loss was alleviated by the ferroptosis inhibitor ferrostatin-1 (Fer-1) (Supplementary Fig. 13g,h), while it was aggravated by HMOX1 overexpression (Supplementary Fig. 14a,b). Knockdown of HMOX1 maintained ΔΨm under both H/R and RSL3 challenges (Supplementary Figs. 15l,m, and 16g,h), suggesting that HMOX1 activation contributes to mitochondrial depolarisation in a stress-dependent manner. Importantly, OAM treatment effectively restored ΔΨm in H/R-injured neurons (Supplementary Fig. 17a,b),

in parallel with the suppression of HMOX1 activation.

These findings align well with our observations of mitochondrial Fe^{2+} accumulation and lipid peroxidation, supporting a mechanistic cascade in which HMOX1-mediated iron dyshomeostasis promotes lipid peroxidation, mitochondrial dysfunction, and neuronal injury, and in which OAMs interrupt this process. The corresponding data and detailed descriptions have been incorporated into the revised manuscript (Lines 466-468; 495-496; 515; 524-525; 615-617).

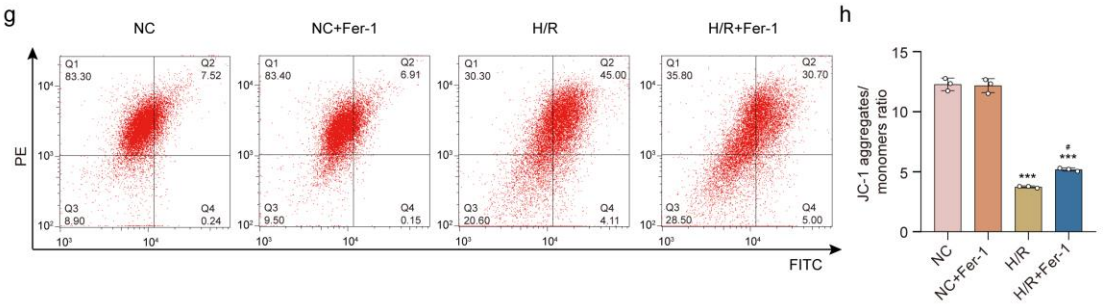

Supplementary Fig. 13g,h | Representative flow cytometry dot plots (**g**) and quantification (**h**) of mitochondrial membrane potential (ΔΨm) assessed by JC-1 staining. JC-1 forms red-fluorescent aggregates in mitochondria with intact ΔΨm and green-fluorescent monomers upon depolarisation. ΔΨm changes are expressed as the JC-1 aggregate/monomer ratios. Fer-1 dose, 5 μM. $n = 3$ biological replicates. Data are presented as mean ± SD. Statistical significance was determined by one-way ANOVA with Tukey's post hoc test (multiple groups). $^{***}P < 0.001$ vs. NC; $^{\#}P < 0.05$, $^{\#\#}P < 0.01$, $^{\#\#\#}P < 0.001$ vs. H/R.

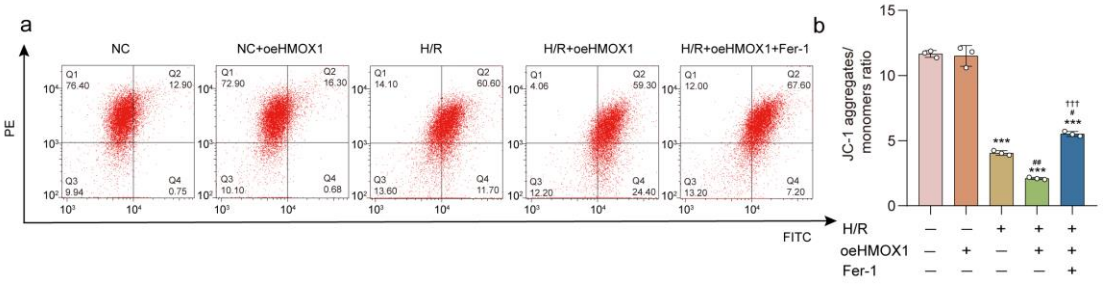

Supplementary Fig. 14a,b | Representative flow cytometry dot plots (**a**) and quantification (**b**) of ΔΨm assessed by JC-1 staining in control and HMOX1-

overexpressing (oeHMOX1) HT22 cells treated with Fer-1 under H/R conditions for 24 h. Fer-1 dose, 5 μM. n = 3 biological replicates. Data are presented as mean ± SD. Statistical significance was determined by one-way ANOVA with Tukey's post hoc test (multiple groups). ***P < 0.001 vs. NC; $^{\#}P$ < 0.05 vs. H/R; $^{\dagger}P$< 0.05 vs. H/R+oeHMOX1.

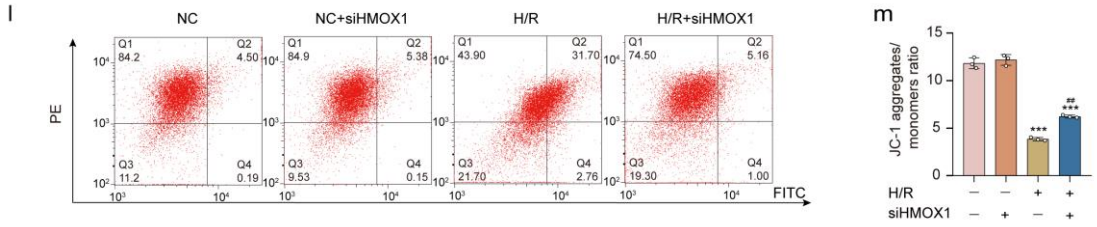

Supplementary Fig. 15l,m | Representative JC-1 flow cytometry dot plots (**l**) and quantification (**m**) of mitochondrial membrane potential in siNC and siHMOX1 cells after 24 h of H/R, expressed as the JC-1 aggregate/monomer ratios. n = 3 biological replicates. Data are presented as mean ± SD. Statistical significance was determined by one-way ANOVA with Tukey's post hoc test (multiple groups). ***P < 0.001 vs. NC; $^{\#}P$ < 0.05 vs. H/R.

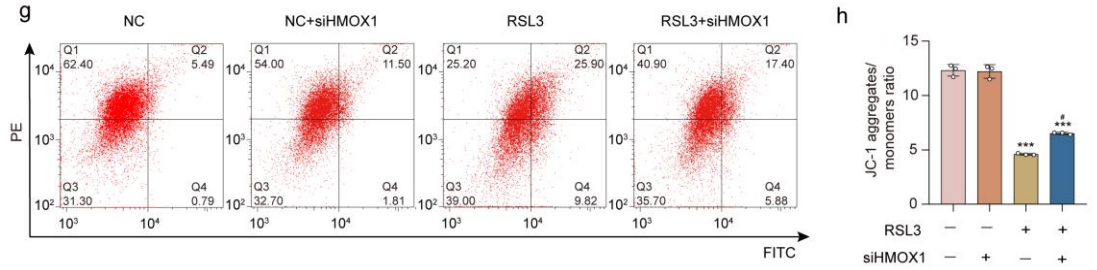

Supplementary Fig. 16g,h | Representative JC-1 flow cytometry dot plots (**g**) and quantification of mitochondrial membrane potential (**h**) in siNC and siHMOX1 cells after 24 h of RSL3 exposure. RSL3 dose, 150 nM. n = 3 biological replicates. Data are presented as mean ± SD. Statistical significance was determined by one-way ANOVA with Tukey's post hoc test (multiple groups). ***P < 0.001 vs. NC; $^{\#}P$ < 0.05 vs. RSL3.

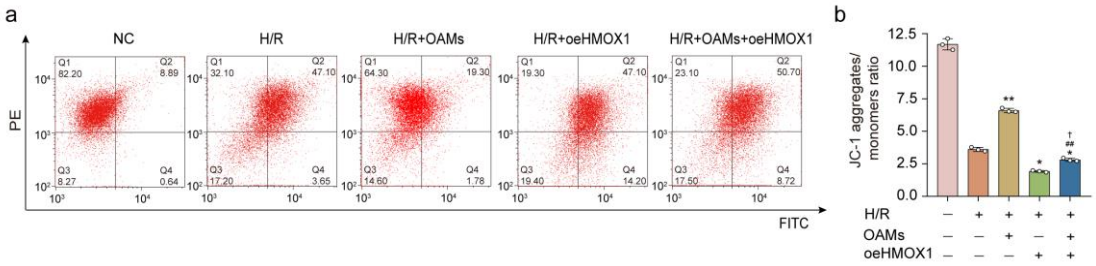

Supplementary Fig. 17a,b | Representative JC-1 flow cytometry dot plots (**a**) and quantification of mitochondrial membrane potential (**b**) in control and oeHMOX1 HT22 cells treated with OAMs under H/R conditions for 24 h. Art-equivalent dose, 250 nM. n = 3 biological replicates. Data are presented as mean ± SD. Statistical significance was determined by one-way ANOVA with Tukey's post hoc test (multiple groups). $^{*}P < 0.05$, $^{***}P < 0.001$ vs. H/R; $^{\#}P < 0.05$ vs. H/R+OAMs; $^{\dagger\dagger}P < 0.01$ vs. H/R+oeHMOX1.

Comment 14: In the descriptions on lines 430 - 432 of the text, it is pointed out that the overexpression of HMOX1 abolished the cytoprotective effect of OAMs and re-induces ferroptosis in the cytoplasm and mitochondria. Then it is also stated that even in the case of HMOX1 overexpression, the combined treatment of OAMs largely restores the levels of ferroptosis markers. There is a contradiction between these two sentences, and it is recommended to make revisions.

Author's response: Thank you for pointing out this inconsistency. We agree that the previous wording was ambiguous and could be interpreted as contradictory.

To clarify our findings: although HMOX1 overexpression clearly aggravates H/R-induced ferroptosis, it does not abolish the cytoprotective effects of OAMs. Rather, even under conditions of enforced HMOX1 upregulation, OAM treatment still attenuates ferroptotic injury by dampening HMOX1-driven signalling and normalising downstream ferroptosis markers, including Fe^{2+} accumulation, lipid ROS, MDA, and GPX4/FTH1/ACSL4 expression patterns.

To more accurately reflect these data and avoid overstating the impact of HMOX1 overexpression, we have revised the relevant sentences in the manuscript as follows:

"Even with HMOX1 overexpression, which worsened H/R-induced injury, OAMs still

exhibited substantial anti-ferroptotic effects. Despite excessive HMOX1 activity, OAM treatment significantly counteracted the biochemical and mitochondrial abnormalities (Fig. 9a–f; Supplementary Fig. 17a, b) and largely normalised the expression of ferroptosis-related proteins, including the upregulation of GPX4 and FTH1 and the suppression of ACSL4 (Supplementary Fig. 17c–f).”

This revision has been incorporated into the revised manuscript (Lines 613-619) to ensure that the text is fully aligned with the experimental results.

Comment 15: The text mentions multiple times that micelles accumulate in microglia, and microglia are involved in I/R-induced brain injury. However, the entire article does not conduct research on OAMs in aspects such as microglia and neuroinflammation. Please supplement relevant experiments to make the article more substantial.

Author's response: Thank you for this important and constructive comment. We fully agree that, given the prominent role of microglia in I/R-induced neuroinflammation and neuronal injury, it is essential to substantiate the effects of OAMs on microglial function. In response, we have added a series of *in vitro* and *in vivo* experiments focusing on microglial uptake and inflammatory responses.

First, we assessed micelle internalisation in BV2 microglial cells using OPDEA-^{Cy5}PCL and PEG-^{Cy5}PCL micelles. Confocal imaging and flow cytometry revealed that OPDEA-^{Cy5}PCL micelles exhibited significantly higher uptake in BV2 cells than PEGylated counterparts (Supplementary Fig. 4a,f,g), consistent with the enhanced membrane engagement conferred by the OPDEA corona. As BV2 microglia possess intrinsic phagocytic activity, they also internalised PEGylated micelles to a greater extent than non-phagocytic endothelial and neuronal cells, which explains the relatively elevated Cy5 signal in the PEG control group. Second, we characterised exocytosis kinetics in BV2 cells and observed that BV2 cells displayed a cumulative exocytosis rate of ~64.0% by 12 h (Supplementary Fig. 4k, l). Third, we examined the impact of OAMs on microglial inflammatory signalling and phenotype under H/R challenge. In BV2 cells, OAM treatment significantly reduced *Tnf* and *Il1b* mRNA levels and decreased secreted TNF-α and IL-1β protein compared with H/R controls

(Supplementary Fig. 6a-d), indicating attenuation of microglia-driven cytokine release. In parallel, immunofluorescence staining for iNOS (M1 marker) and Arg1 (M2 marker) demonstrated that OAMs suppressed H/R-induced M1 polarisation while promoting a shift towards a reparative M2 phenotype (Supplementary Fig. 6e,h).

These data show that OAMs not only reach and are efficiently internalised by microglia but also directly modulate microglial activation and neuroinflammatory output, thereby complementing their ferroptosis-inhibitory effects in neurons. All new experimental results and the corresponding text have been incorporated into the revised manuscript (Lines 215-218; 278-280; 345-358).

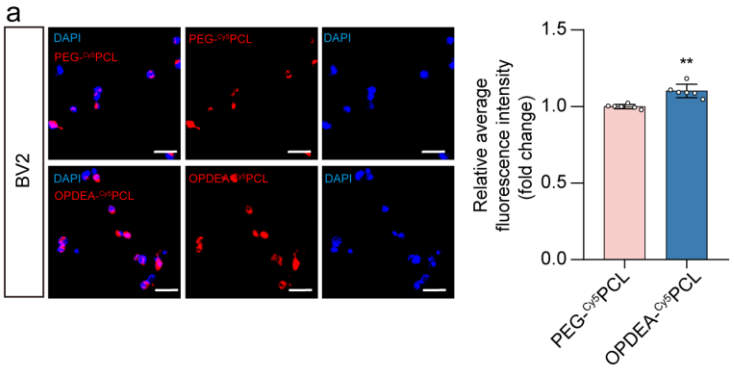

Supplementary Fig. 4a | Confocal microscopy images (left) and quantitative analysis (right) of cellular uptake of Cy5-labelled OPDEA–PCL micelles by BV2 microglial cells after 24 h incubation (n = 6 biological replicates). Nuclei were stained with DAPI (blue). Cy5-equivalent dose, 0.5 μg ml^{-1}. Scale bar, 20 μm. Data are presented as mean ± SD. Statistical significance was determined by a two-tailed unpaired Student's t test. $^{**}P < 0.01$.

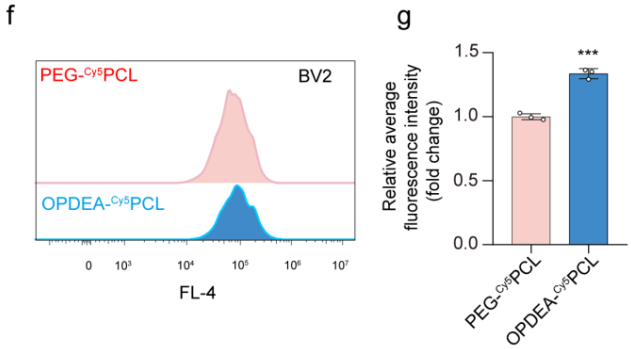

Supplementary Fig. 4f,g | Representative flow cytometry histograms (**f**) and corresponding quantification (**g**) of Cy5-labelled micelle uptake in BV2 microglial cells after 24 h incubation (n = 3 biological replicates). Cy5-equivalent dose, 0.5 µg ml^{-1}. Data are presented as mean ± SD. Statistical significance was determined by a two-tailed unpaired Student's t test. ***$P < 0.001$.

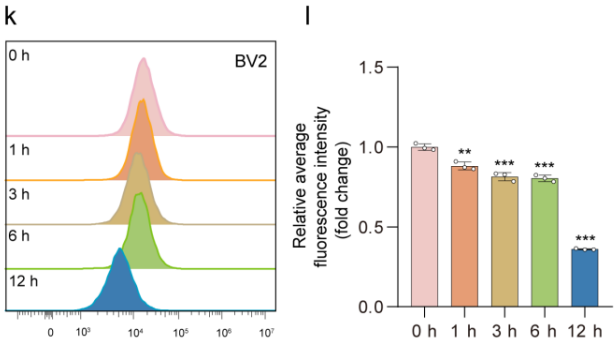

Supplementary Fig. 4k,l | Representative flow cytometry histogram (**k**) and quantification (**l**) of time-dependent exocytosis of OPDEA–^{Cy5}PCL micelles from BV2 microglial cells. Cells were pre-incubated with micelles for 24 h, washed, and transferred to fresh medium for the indicated durations (n = 3 biological replicates). Cy5-equivalent dose, 0.5 µg ml^{-1}. Data are presented as mean ± SD. Statistical significance was determined by one-way ANOVA with Dunnett's multiple comparison test (multiple groups). **$P < 0.01$, ***$P < 0.001$.

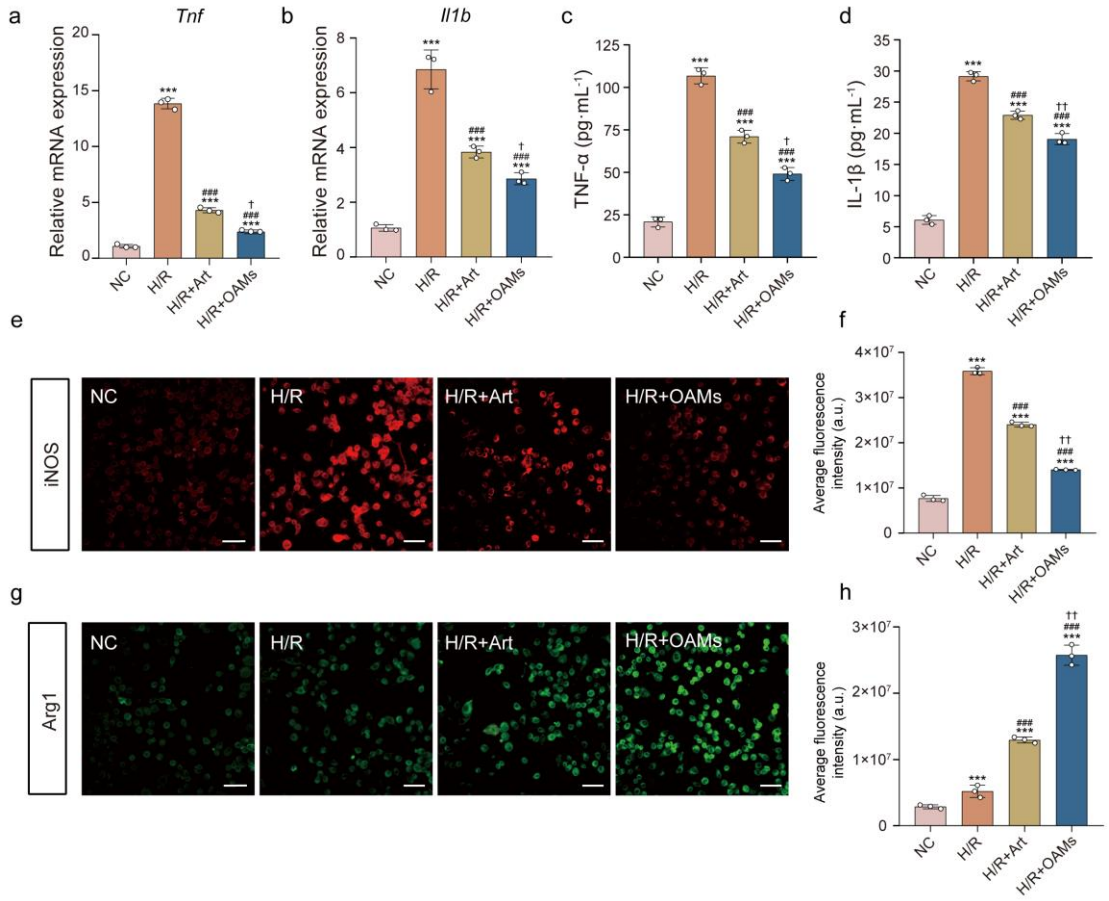

Supplementary Fig. 6 | OAMs attenuate microglial inflammation and reprogramme microglial polarisation. a–d, Relative mRNA expression of *Tnf* (**a**) and *Il1b* (**b**) in BV2 microglial cells treated with OAMs for 24 h under hypoxia–reoxygenation (H/R), as assessed by qRT–PCR; corresponding TNF-α (**c**) and IL-1β (**d**) protein levels in culture supernatants measured by ELISA (n = 3 biological replicates). Art-equivalent dose, 250 nM. **e–h**, Immunofluorescence images of BV2 cells stained for the M1 marker iNOS (red) and M2 marker Arg1 (green) after 24 h of H/R with or without OAMs (**e, g**), and quantification of iNOS (**f**) and Arg1 (**h**) fluorescence intensity (n = 3 biological replicates). Art-equivalent dose, 250 nM. Scale bar, 100 μm. Data are presented as mean ± SD. Statistical significance was determined by one-way ANOVA with Tukey's post hoc test (multiple groups). $^{***}P < 0.001$ vs. NC; $^{\#}P < 0.05$, $^{\#\#}P < 0.01$, $^{\#\#\#}P < 0.001$ vs. H/R; $^{\dagger}P < 0.05$, $^{\dagger\dagger}P < 0.01$ vs. H/R+Art.

Comment 16: Some writing formats in the text are incorrect. When an abbreviation appears for the first time, the full name should be written. For example, in the Abstract

section, the full name of CNS was not written when it first appeared. Please check and revise the entire text.

Author's response: Thank you for this helpful suggestion. We have now added the full term “central nervous system (CNS)” at its first occurrence in the Abstract (Line 38). In addition, we have thoroughly reviewed the entire manuscript to ensure that all abbreviations are introduced with their full names upon first use.

Comment 17: In the text, the dosage unit is sometimes written as μg/mL and sometimes as μg mL^{-1}. Please unify the writing according to the requirements.

Author's response: Thank you for this helpful suggestion. We have carefully checked the entire manuscript and standardised all concentration and dosing units to the format "μg mL^{-1}".

Comment 18: Some pictures are not in standard format. For example, the description of the x-axis in Fig 2D is not aligned with the axis. Please check and revise the whole text.

Author's response: Thank you for your valuable suggestion. We have corrected the x-axis formatting in Fig. 2d so that the time labels are now properly aligned with the axis. We also reviewed all figures and adjusted any non-standard graphical elements to comply with the journal’s formatting guidelines.

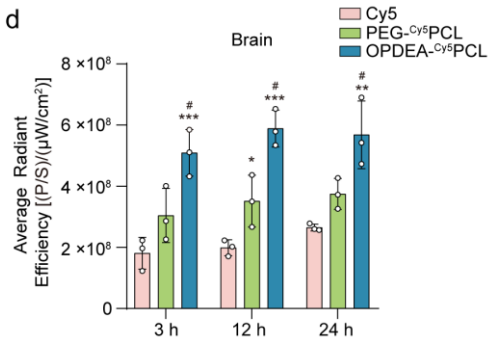

Fig. 2d | Quantitative analysis of Cy5 fluorescence in whole-brain tissues collected at the indicated time points after *i.v.* administration of free Cy5, PEG-^{Cy5}PCL, or OPDEA-^{Cy5}PCL micelles in mice (n = 3). Cy5-equivalent dose, 100 μg kg^{-1}. Data are presented

as mean ± SD. Statistical significance was determined by one-way ANOVA with Tukey's post hoc test (multiple groups). *$P < 0.05$, **$P < 0.01$, ***$P < 0.001$ vs. Cy5; $^{\#}P < 0.05$ vs. PEG-^{Cy5}PCL.

Reviewer 3

In this manuscript, Zhang et al. present a novel nanotherapeutic platform (OAMs) to mitigate post-resuscitation brain injury. The platform enhances blood-brain barrier (BBB) penetration of artesunate using zwitterionic OPDEA micelles that facilitate adsorptive-mediated transcytosis. This receptor-independent mechanism represents a significant advance over conventional delivery methods. The neuroprotective efficacy of OAMs was validated through comprehensive assessments in a murine CA/CPR model. Furthermore, the study elucidates a key molecular mechanism, demonstrating that OAMs exert their therapeutic effect by inhibiting heme oxygenase-1 (HMOX1)-mediated ferroptosis. However, several concerns need to be addressed before the manuscript can be accepted for publication.

Author's response: Thank you for your positive assessment of our work. We greatly appreciate your recognition of the mechanistic insights and therapeutic potential of our nanoplatform, as well as your constructive feedback that has significantly enhanced the quality of the manuscript.

Comment 1: In Figure 1B, please label the pink cells located within the blood vessel.

Author's response: Thank you for this valuable suggestion. We have labelled the pink cells within the vessel as "vascular endothelial cells", updated the figure panel and its legend to reflect this change.

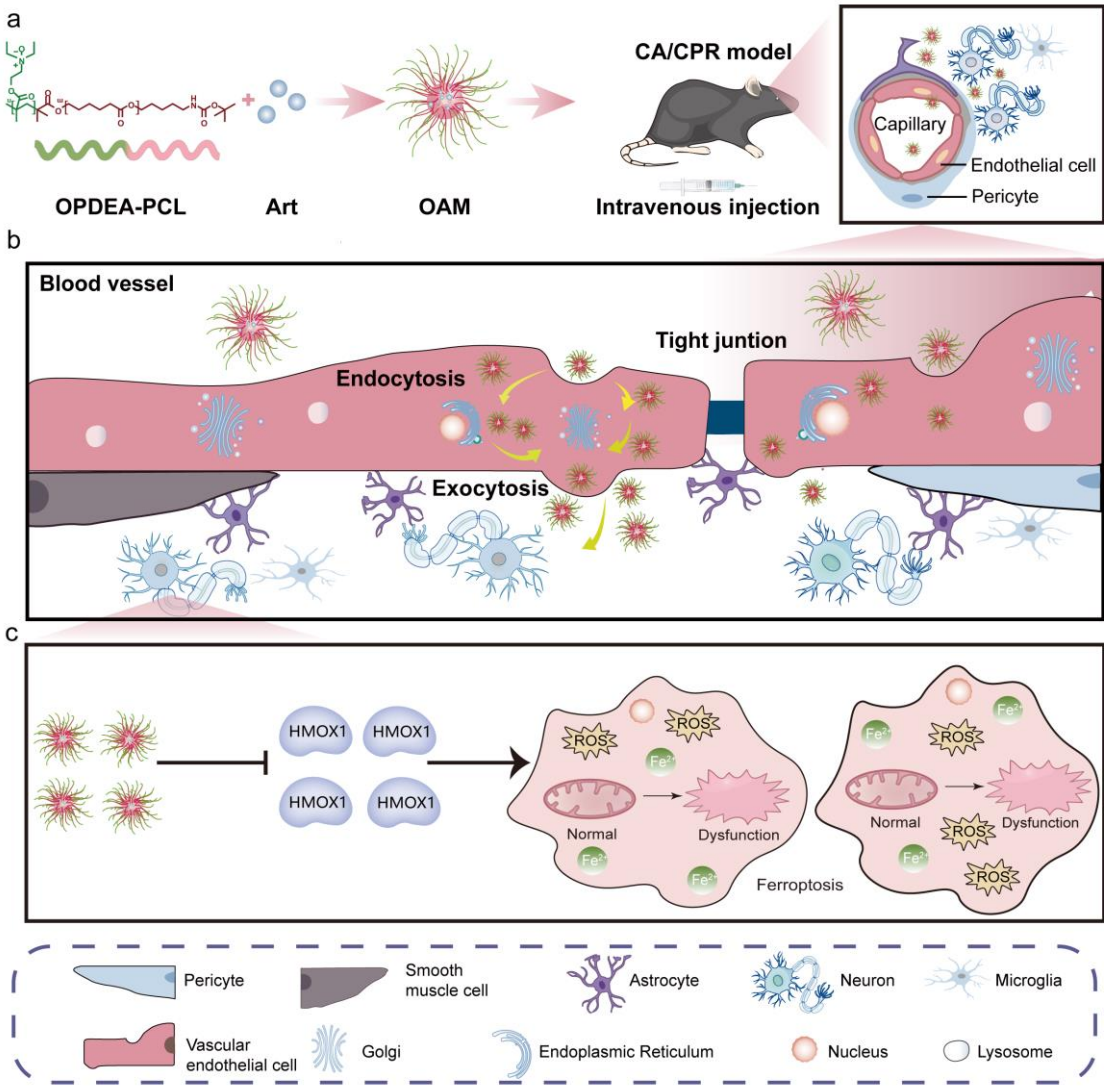

Fig. 1 | Schematic illustration of OAMs for targeted neuroprotection after CA. a, Art is encapsulated into the zwitterionic block copolymer OPDEA-PCL to form well-defined OPDEA-based Art-loaded micelles (OAMs). **b**, Following intravenous (*i.v.*) administration, OAMs bind to brain microvascular endothelial cells and undergo AMT, thereby traversing the intact BBB. **c**, In the brain parenchyma, OAMs accumulate in hippocampal neurons and microglia, where they inhibit HMOX1-mediated ferroptosis, restore iron homeostasis, and attenuate I/R injury after CA and CPR.

Comment 2: Figure S1B is not referenced in the results section.

Author's response: Thank you for your careful observation.

The data from Supplementary Fig. 1b (now updated as Supplementary Fig. 2c) are now explicitly cited in the Results section of the main text (Lines 134-136):

"The micelles exhibited a drug loading content (DLC) of 7.0% and a drug loading efficiency (DLE) of 75.4% (Supplementary Fig. 2c)."

Comment 3: Please clarify how it was determined that OAMs substantially prolonged drug circulation, and explain the calculation that shows 34.3% of the dose was retained at the specified time point.

Author's response: Thank you for this thoughtful comment. We have clarified both the experimental basis for determining that OAMs prolong systemic circulation and the method used to derive the dose-retention percentage.

(1) Basis for concluding that OAMs prolong drug circulation

To more transparently depict the pharmacokinetic behaviour of OAMs, we re-plotted the concentration-time curve in Fig. 1a with the Y-axis normalised to the initial blood concentration (C_0). Quantitatively, OAMs exhibited a markedly prolonged half-life (38.9 min) compared with free Art, and at 1 h post-injection, 10.2 ± 1.4% of the initial dose remained in the blood for OAMs versus 2.7 ± 0.54% for free Art. Consistently, the $AUC_{0\text{-}1h}$ of OAMs was 114.2 ID%·h·mL^{-1}, 2.44-fold higher than that of free Art (46.8 ID%·h·mL^{-1}) (Fig. 2a,b). These pharmacokinetic parameters indicate that OAMs substantially enhance systemic exposure relative to free drug.

(2) Calculation of dose retention at the specified time point

The percentage of dose retained in circulation at a given time (t) was calculated as:

$$\text{Residual rate } (\%) = C_t / C_0 \times 100\%,$$

where C_0 is the initial blood concentration immediately after administration, and C_t is the measured concentration at time t. The previously reported value of 34.3% was a result of miscalculation. We sincerely apologize for this oversight. Applying the correct calculation, we determined the residual fraction at 1 h for OAMs to be 10.2 ± 1.2%.

We have updated the manuscript to reflect this correction and ensured consistency with the normalised pharmacokinetic plots (Lines 144-150).

a

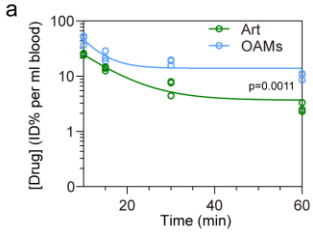

b

Parameters	T_{max}(min)	C_{max}(μg·mL^{-1})	$AUC_{(0-t)}$(μg·mL^{-1}·min)	$T_{1/2z}$(min)	$MRT_{(0-t)}$(min)	CL(mL·kg^{-1}·min^{-1})
Art	10.00 ± 0.00	1.25 ± 0.05	46.80 ± 0.26	20.30 ± 4.93	11.60 ± 0.96	98.4 ± 2.8
OAMs	10.00 ± 0.00	2.33 ± 0.45	114.20 ± 41.7	38.90 ± 5.56	6.28 ± 7.53	36.4 ± 6.8

Fig. 2a,b | Plasma concentration–time profiles expressed as percentage of injected dose per millilitre of blood (%ID ml^{-1}) (**a**) and corresponding pharmacokinetic parameters (**b**) of free Art and OAMs following a single *i.v.* injection in rats (n = 3). Art-equivalent dose, 5 mg kg^{-1}.

Comment 4: Please check the time label in Figure 2D.

Author's response: Thank you for your suggestion. We have corrected the time labels in Fig. 2d to ensure that they are properly aligned with the x-axis and clearly correspond to the plotted data.

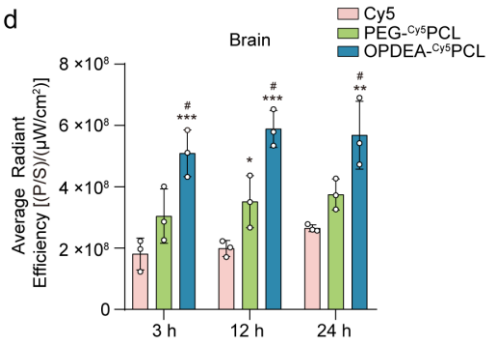

Fig. 2d | Quantitative analysis of Cy5 fluorescence in whole-brain tissues collected at the indicated time points after *i.v.* administration of free Cy5, PEG-^{Cy5}PCL, or OPDEA-^{Cy5}PCL micelles in mice (n = 3). Cy5-equivalent dose, 100 μg kg^{-1}. Data are presented as mean ± SD. Statistical significance was determined by one-way ANOVA with Tukey's post hoc test (multiple groups). *P < 0.05, **P < 0.01, ***P < 0.001 vs. Cy5; $^{\#}P$ < 0.05 vs. PEG-^{Cy5}PCL.

Comment 5: In Figures 3A and 3B, the β-actin and Cy5 staining is difficult to discern due to poor image resolution and the low density of the bEnd.3 and HT22 cells.

Author's response: Thank you for pointing out this important issue. In response, we have replaced the original panels with higher-resolution confocal images acquired at increased cell density, thereby improving the visibility of both β-actin and Cy5 signals in bEnd.3 and HT22 cells. The revised images provide clearer delineation of cellular morphology and micelle distribution and have been incorporated into the updated manuscript (Fig. 3a,b).

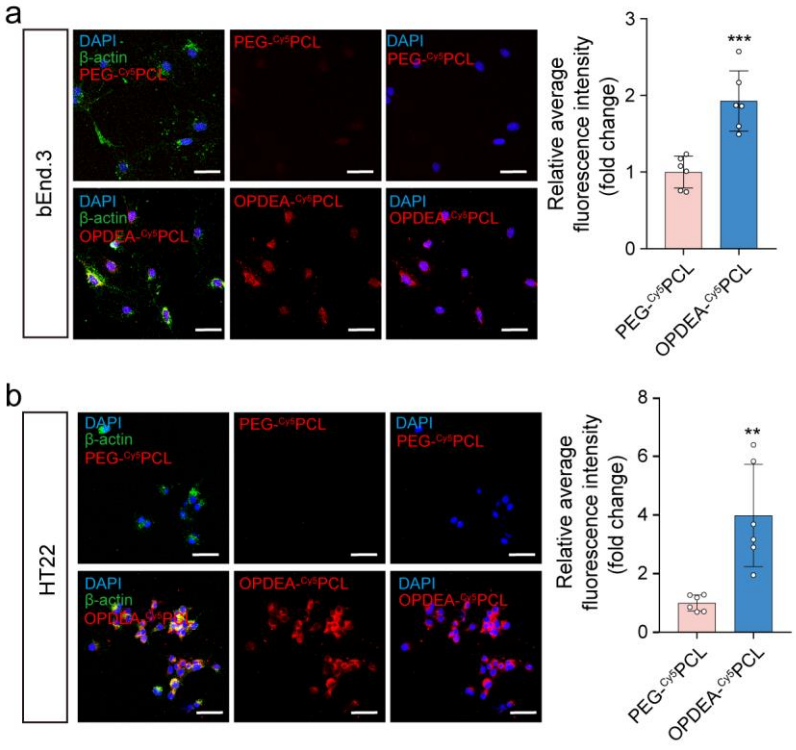

Fig. 3a,b | Confocal microscopy images (left) and quantitative analyses (right) of Cy5-labelled micelle uptake in bEnd.3 endothelial cells (**a**) and HT22 neuronal cells (**b**) after 24 h incubation ($n = 6$ biological replicates). The cytoskeleton was visualised by β-actin staining (green), and nuclei were stained with DAPI (blue). Cy5-equivalent dose, 0.5 μg ml^{-1}. Scale bar, 20 μm. Data are presented as mean ± SD. Statistical significance was determined by two-tailed unpaired Student's *t* test (two groups). $^{**}P < 0.01$, $^{***}P < 0.001$ vs. PEG-^{cy5}PCL .

Comment 6: The resolution of Figure 3K is poor. Please provide a higher-resolution version.

Author's response: Thank you for your valuable suggestion. We have now replaced Fig. 3k with a higher-resolution image to improve clarity of cellular morphology and Cy5 fluorescence. The improved panel has been included in the revised manuscript (Fig. 3k).

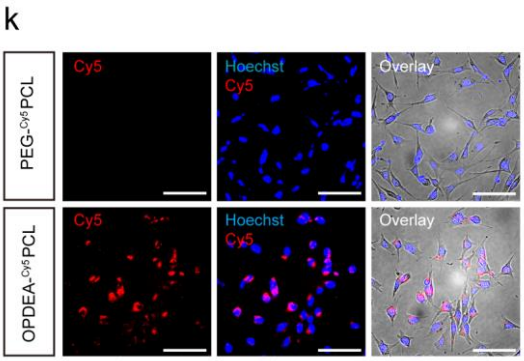

Fig. 3k | Inverted fluorescence microscopy images of Cy5 signals in HT22 cells located in the basolateral chamber after 24 h transcytosis. Nuclei were stained with Hoechst (blue). Cy5-equivalent dose, 0.5 μg ml^{-1}. Scale bar, 100 μm.

Comment 7: In Figures 4D i and 4D ii, the cell counts in the flow cytometry plots are too small to read. Please enlarge them. In the legend for Figure 4, please define the symbols (*, #, †) used in the bar chart. Annexin-V staining detects apoptosis, whereas this study focuses on ferroptosis. The authors are suggested use a different method to assess cell viability, such as a WST assay.

Author's response: Thank you for these valuable and constructive suggestions regarding Fig. 4 and the associated assays. We have carefully addressed each point as follows:

First, to improve the readability of the flow cytometry data, we increased the font size of the cell count values in the scatter plots (now shown in Fig. 4e).

Second, we have revised the legend of Fig. 4 to explicitly define all statistical symbols used in the bar graphs: $^{*}P < 0.05$, $^{**}P < 0.01$, $^{***}P < 0.001$ vs. NC; $^{\#}P < 0.05$, $^{\#\#}P < 0.01$, $^{\#\#\#}P < 0.001$ vs. H/R; $^{\dagger}P < 0.05$, $^{\dagger\dagger}P < 0.01$ vs. H/R+Art.

Third, we fully agree that Annexin V staining primarily reflects apoptotic cell death, whereas the central focus of this study is ferroptosis. In line with the reviewer's

recommendation, we have supplemented the viability assessment with a CCK-8 assay (a WST-type metabolic viability assay). Under H/R conditions, OAMs significantly improved neuronal viability compared with free Art, as shown in Fig. 4c. The Annexin V data are retained as supportive evidence of reduced apoptosis, but our main conclusions regarding cell viability now rely on the CCK-8 results.

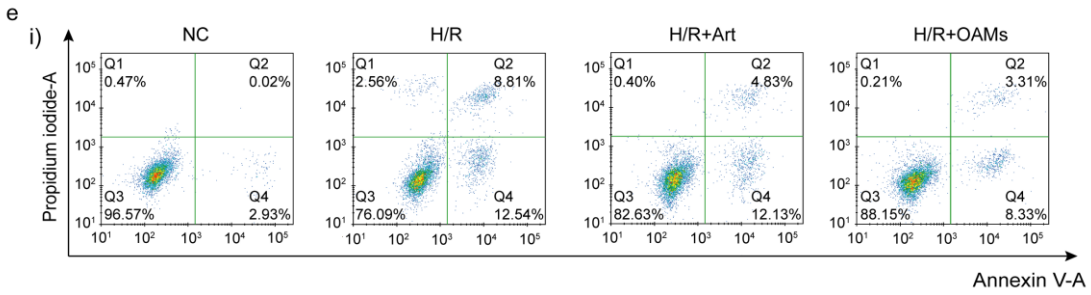

Fig. 4e | Flow cytometric assessment of (**i**) apoptotic cell populations and (**ii**) intracellular ROS levels in HT22 cells treated with OAMs under H/R conditions for 24 h (n = 3 biological replicates). Art-equivalent dose, 250 nM.

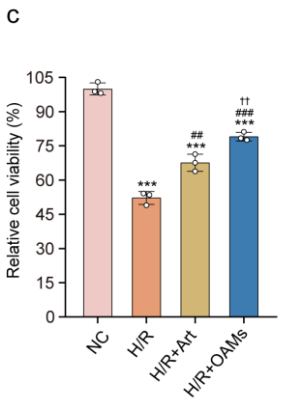

Fig. 4c | Effects of OAMs on cell viability in HT22 cells exposed to H/R for 24 h (n = 3 biological replicates). Art-equivalent dose, 250 nM. Data are presented as mean ± SD. Statistical significance was determined by one-way ANOVA with Tukey's post hoc test (multiple groups). ***$P < 0.001$ vs. NC; $^{\#\#}P < 0.01$, $^{\#\#\#}P < 0.001$ vs. H/R; $^{\dagger\dagger}P < 0.01$ vs. H/R+Art.

Comment 8: To ensure a more direct and accurate comparison for the IHC staining in

Figure 5E, tissue sections should be taken from the same or adjacent regions.

Author's response: Thank you for this valuable suggestion. We fully agree that anatomical consistency is essential for reliable comparison across treatment groups. In response, we have re-acquired all IHC images in Fig. 5f by capturing the same or immediately adjacent hippocampal regions under identical imaging settings. Quantitative analyses were repeated based on these updated sections, and the results remained consistent with our original conclusions. The revised images have now been incorporated into Fig. 5f in the updated manuscript.

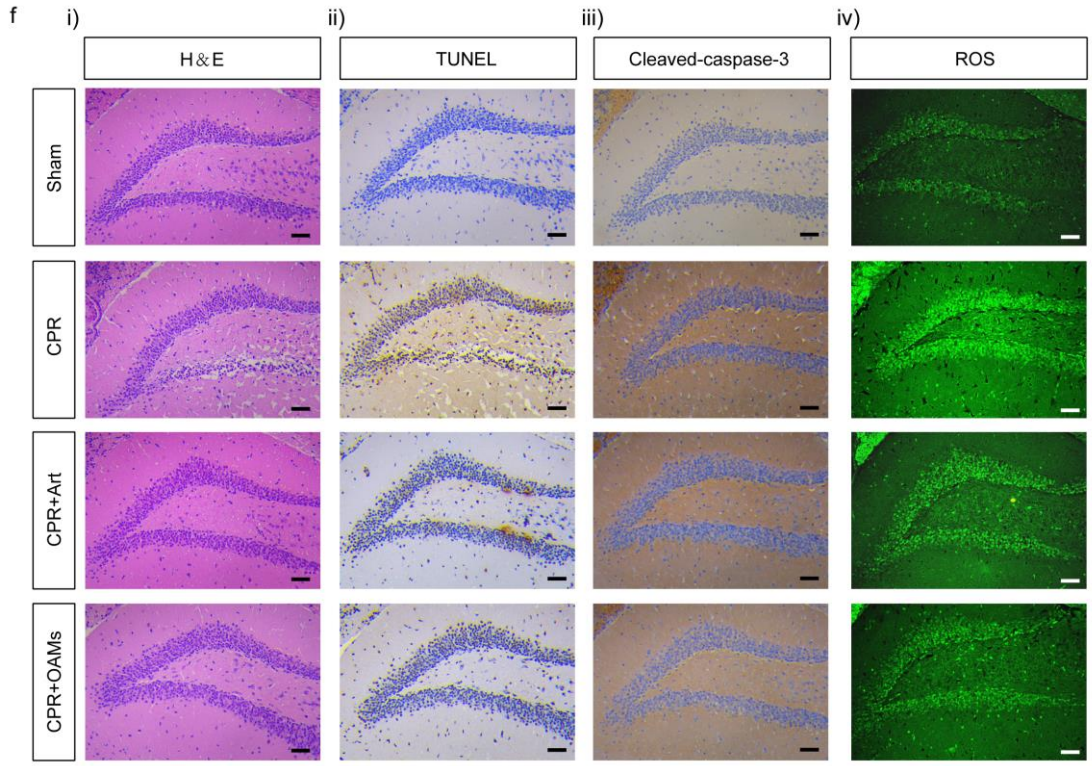

Fig. 5f | Histological assessments of hippocampal injury: (**i**) H&E staining, (**ii**) TUNEL staining of apoptotic cells, (**iii**) immunohistochemical staining of cleaved caspase-3, and (**iv**) ROS detection using 2',7'-dichlorodihydrofluorescein diacetate (DCFH-DA) (n = 6 mice). Scale bar, 100 μm.

Comment 9: Although HMOX1 overexpression (oeHMOX1) enhances H/R-induced ferroptosis (Figure 7A), the data also show that oeHMOX1 alone did not elevate Fe^{2+} levels, whereas H/R stress did (Figures 7B-7J). This suggests that H/R stress promotes

ferroptosis through additional mechanisms independent of HMOX1. Furthermore, while HMOX1 knockdown significantly ameliorated H/R-induced ROS generation and lipid peroxidation, it remains unclear if it can also rescue H/R-inhibited cell viability. I suggest that the authors investigate this. As a control, they should also test whether ferrostatin-1 can inhibit ferroptotic activity and improve the viability of HT22 cells subjected to H/R stress alone, which would also confirm the role of ferroptosis in H/R.

Author's response: Thank you for this insightful and constructive comment. We have now performed additional experiments and expanded our mechanistic explanation to address all aspects of your concerns.

First, as the reviewer correctly notes, although HMOX1 overexpression (oeHMOX1) enhances ferroptosis under H/R conditions, oeHMOX1 alone does not increase Fe^{2+} levels under basal conditions (Fig. 7c). This context-dependent effect aligns with the stress-gated nature of HMOX1-mediated ferroptosis. Under physiological conditions, ferritin (FTH1)-mediated iron sequestration, ferroportin (FPN)-dependent export, and an intact GSH-GPX4 system tightly regulate the labile iron pool, thereby preventing iron-driven lipid peroxidation. Thus, HMOX1 overexpression alone is insufficient to expand the labile iron pool to a ferroptotic threshold. In contrast, H/R stress causes GSH depletion, mitochondrial redox dysregulation, and accumulation of phospholipid radicals, thereby lowering the threshold for Fe^{2+}-dependent lipid peroxidation and unmasking the pro-ferroptotic activity of HMOX1 (*Redox Biol. 2024, 76, 103345*).

Second, to directly assess whether HMOX1 affects neuronal survival under H/R challenge, we conducted additional viability assays. As expected, HMOX1 overexpression further decreased HT22 neuronal viability following H/R (Fig. 7b), whereas HMOX1 knockdown significantly rescued cell viability under identical conditions (Supplementary Fig. 15e). These findings parallel our observations of restored Fe^{2+} homeostasis, reduced lipid peroxidation, and suppressed ROS generation in HMOX1-silenced cells, thereby confirming the functional contribution of HMOX1 to H/R-induced ferroptotic injury.

Third, following your recommendation, we examined whether direct pharmacological inhibition of ferroptosis can rescue neuronal viability after H/R.

Treatment with ferrostatin-1 (Fer-1) significantly improved HT22 viability under H/R stress (Supplementary Fig. 13a) and reduced cytosolic Fe^{2+} levels, lipid peroxidation products, and lipid ROS, while increasing intracellular GSH (Supplementary Fig. 13a–f). These results further validate ferroptosis as a major execution mechanism of H/R-induced neuronal injury.

All newly acquired experimental data and corresponding descriptions have been incorporated into the revised manuscript (Lines 460-471; 513).

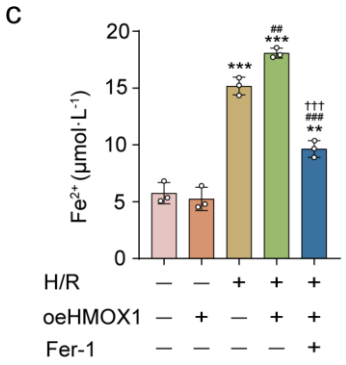

Fig. 7c | Intracellular Fe^{2+} levels determined by the ferrozine colourimetric assay. Fer-1 dose, 5 μM. $n = 3$ biological replicates. Data are presented as mean ± SD. Statistical significance was determined by one-way ANOVA with Tukey's post hoc test (multiple groups). $^{**}P < 0.01$, $^{***}P < 0.001$ vs. NC+oeHMOX1; $^{\#\#}P < 0.01$, $^{\#\#\#}P < 0.001$ vs. H/R; $^{\dagger\dagger\dagger}P < 0.001$ vs. H/R+oeHMOX1.

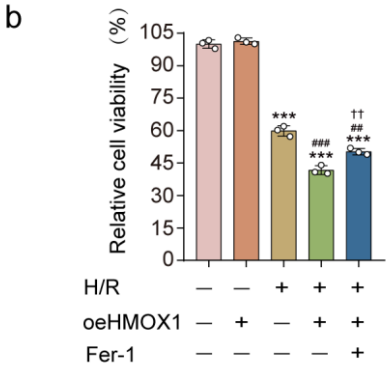

Fig. 7b | Cell viability of normal and oeHMOX1 HT22 cells subjected to H/R for 24 h with or without Fer-1. Fer-1 dose, 5 μM. $n = 3$ biological replicates. Data are presented as mean ± SD. Statistical significance was determined by one-way ANOVA with

Tukey's post hoc test (multiple groups). ***$P < 0.001$ vs. NC+oeHMOX1; $^{\#\#}P < 0.01$, $^{\#\#\#}P < 0.001$ vs. H/R; $^{\dagger\dagger}P < 0.01$ vs. H/R+oeHMOX1.

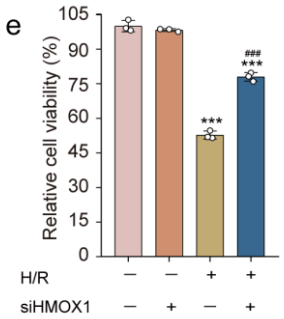

Supplementary Fig. 15e | Cell viability in siNC and siHMOX1 HT22 cells after 24 h of H/R. $n = 3$ biological replicates. Data are presented as mean ± SD. Statistical significance was determined by one-way ANOVA with Tukey's post hoc test (multiple groups). ***$P < 0.001$ vs. NC; $^{\#\#\#}P < 0.001$ vs. H/R.

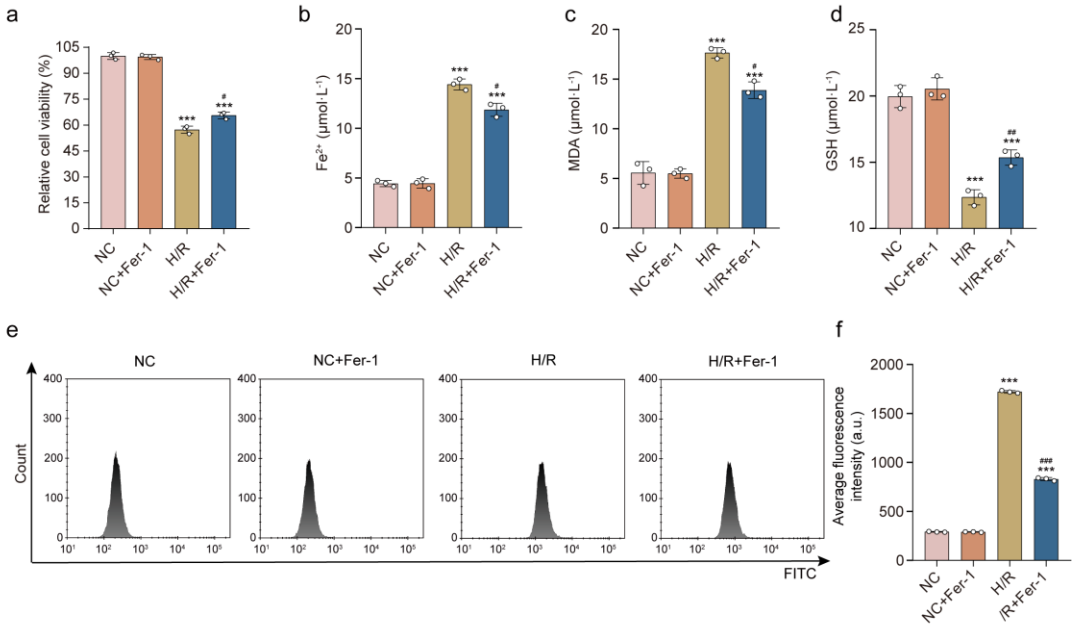

Supplementary Fig. 13a-f | **a**, Cell viability after Fer-1 treatment under H/R for 24 h. **b**, Intracellular Fe^{2+} levels measured by the Ferrozine assay. **c, d**, Levels of malondialdehyde (MDA, c) and glutathione (GSH, d) assessed by thiobarbituric acid (TBA) colourimetry and 5,5'-dithiobis-(2-nitrobenzoic acid) (DTNB) assays, respectively. **e, f**, Representative flow cytometry histograms (**e**) and quantification (**f**)

of cytosolic lipid ROS using C11-BODIPY 581/591 probe. Fer-1 dose, 5 μM. $n = 3$ biological replicates. Data are presented as mean ± SD. Statistical significance was determined by one-way ANOVA with Tukey's post hoc test (multiple groups). ***$P < 0.001$ vs. NC; $^{\#}P < 0.05$, $^{\#\#}P < 0.01$, $^{\#\#\#}P < 0.001$ vs. H/R.

Comment 10: Based on the western blots in Figure S6A, the knockdown efficiency is not clear. Please provide quantification of the blot results. In Figure S6, RSL3 was applied to HT22 cells *in vitro*. Therefore, the dose should be reported in units of concentration (e.g., μM, nM) rather than mg/kg, which is an *in vivo* dosage unit.

Author's response: Thank you for these valuable suggestions. In response, we have clarified the siRNA knockdown efficiency. Western blot band intensities were quantified using ImageJ and normalised to GAPDH, and the results are presented in Supplementary Fig. 15b. Among the three candidates, siHMOX1-1 exhibited the greatest knockdown efficiency and was therefore selected for subsequent experiments; its silencing efficacy has been further validated at protein levels in HT22 cells (Supplementary Fig. 15c,d).

In addition, we appreciate the reviewer's careful observation regarding the dosing unit of RSL3 in the *in vitro* experiments. We have corrected this and now report the RSL3 dose as a concentration (150 nM) rather than mg kg^{-1}, in line with standard *in vitro* ferroptosis protocols *(J. Hazard. Mater., 2025, 488, 137374)*.

These revisions have been incorporated into the updated manuscript (Lines 510-512; 1089-1090).

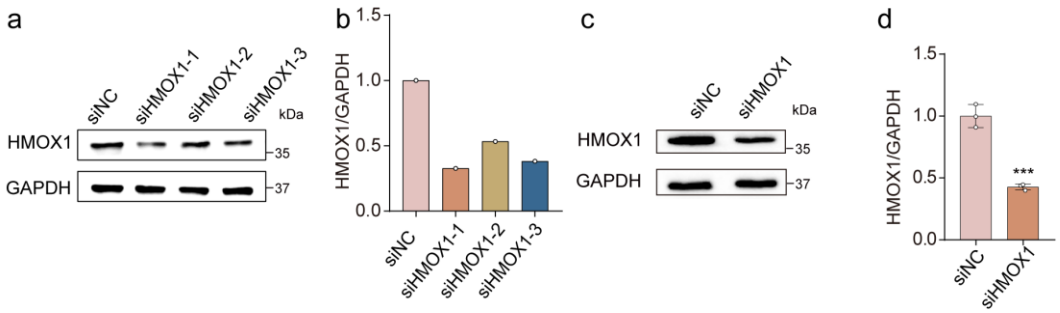

Supplementary Fig. 15a-d | a, b, Representative western blots (**a**) and quantification

(**b**) of HMOX1 protein levels in HT22 cells transfected with non-targeting control siRNA (siNC) or three HMOX1-targeting siRNAs (siHMOX1-1, siHMOX1-2, siHMOX1-3) under basal conditions. **c, d**, Validation of the selected siRNA (siHMOX1; the sequence showing the greatest knockdown in **a, b**) by western blot (**c**) and densitometric analysis (**d**) of HMOX1 in siNC and siHMOX1 cells. $n = 3$ biological replicates. Data are presented as mean ± SD. Statistical significance was determined by a two-tailed unpaired Student's *t* test (two groups). ***$P < 0.001$ vs. siNC.

Comment 11: Regarding lines 397-399, the authors state that RSL3 treatment reverses the protective effect of HMOX1 shRNA, thereby confirming the role of HMOX1. This reasoning is questionable because RSL3 is a direct inducer of ferroptosis. Furthermore, a control group showing the effect of RSL3 alone is missing and should be included.

Author's response: Thank you for this insightful and important comment. We agree that our original interpretation was flawed, as RSL3 is a direct GPX4 inhibitor and potent ferroptosis inducer; therefore, using RSL3 to "reverse" the effects of HMOX1 knockdown does not logically validate HMOX1's role in the pathway.

To rigorously clarify the contribution of HMOX1 to ferroptosis, we conducted an additional set of mechanistic experiments that included a proper RSL3-alone control group. The newly added experimental design includes the following groups: Control, RSL3, RSL3+siNC, and RSL3+siHMOX1 (Supplementary Fig. 16). This framework allowed us to test whether HMOX1 knockdown modulates ferroptosis triggered directly by GPX4 inhibition, independent of H/R-induced stress. The results demonstrate that HMOX1 knockdown significantly alleviated RSL3-induced ferroptotic injury, as evidenced by reduced lipid ROS and MDA accumulation and by restored GPX4 and FTH1 expression, closely paralleling the protective effects observed in the H/R model. These findings reinforce that HMOX1 functions as an upstream amplifier of ferroptotic signalling across distinct ferroptosis induction pathways.

All newly added experimental data and revised interpretations have been incorporated into the updated manuscript (Lines 519-531). We sincerely appreciate the reviewer's comment, which has helped strengthen the mechanistic clarity and validity

of our study.

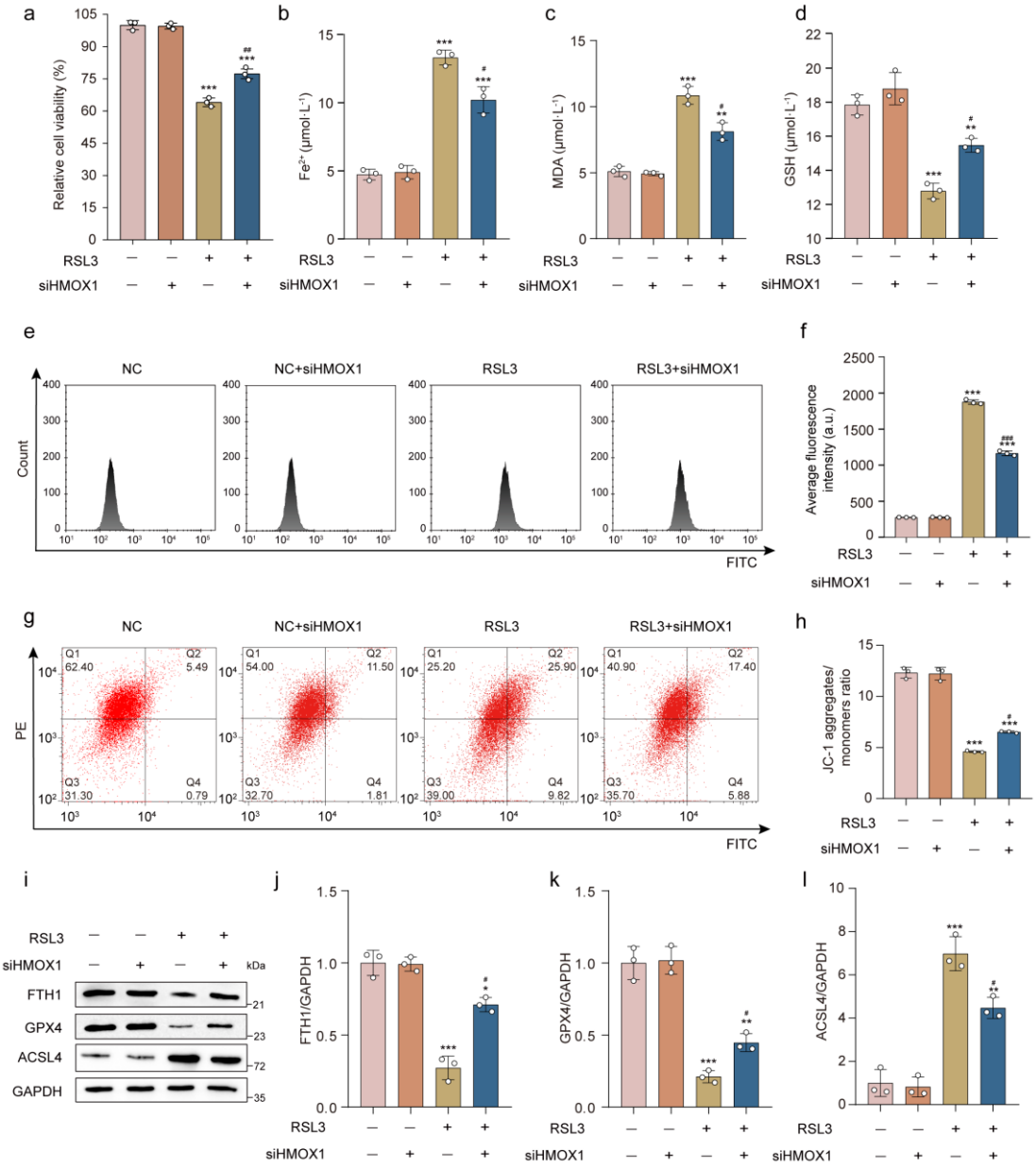

Supplementary Fig. 16 | HMOX1 knockdown attenuates RSL3-induced ferroptosis in HT22 neurons. a–d, Cell viability (**a**, CCK-8 assay), cytosolic Fe^{2+} levels (**b**, ferrozine assay), MDA levels (**c**, TBA method), and GSH content (**d**, DTNB method) in siNC and siHMOX1 HT22 cells treated with RSL3 for 24 h under basal culture conditions. **e, f**, Representative flow cytometry histograms (**e**) and quantification (**f**) of cytosolic lipid ROS in siNC and siHMOX1 cells following 24 h of RSL3 treatment, detected using C11-BODIPY 581/591. **g, h**, Representative JC-1 flow cytometry dot plots (**g**) and quantification of mitochondrial membrane potential (**h**) in

siNC and siHMOX1 cells after 24 h of RSL3 exposure. **i–l**, Representative western blots (**i**) and relative expression of FTH1 (**j**), GPX4 (**k**), and ACSL4 (**l**) in siNC and siHMOX1 cells treated with RSL3 for 24 h, with GAPDH as loading control. RSL3 dose, 150 nM. $n = 3$ biological replicates. Data are presented as mean ± SD. Statistical significance was determined by one-way ANOVA with Tukey's post hoc test (multiple groups). $^{*}P < 0.05$, $^{**}P < 0.01$, $^{***}P < 0.001$ vs. NC; $^{\#}P < 0.05$, $^{\#\#}P < 0.01$, $^{\#\#\#}P < 0.001$ vs. RSL3.

Comment 12: Do H/R and CPR increase the protein expression of HMOX1? Does OAM treatment decrease HMOX1 expression? What is the potential mechanism for upregulating HMOX1?

Author's response: Thank you for this insightful comment. In response, we have conducted additional experiments and expanded the mechanistic discussion to address all three aspects in detail.

(1) Do H/R and CPR increase the protein expression of HMOX1?

Yes. We now provide protein-level evidence that both *in vitro* H/R and *in vivo* CPR robustly upregulate HMOX1. Western blot analyses of H/R-challenged HT22 neurons and hippocampal tissue from CA/CPR mice demonstrated a significant increase in HMOX1 protein expression compared with their respective controls (Fig. 6h,i). These findings indicate that HMOX1 is a stress-responsive enzyme induced by global I/R conditions, likely reflecting the integrated impact of oxidative stress and neuroinflammatory signaling.

(2) Does OAM treatment decrease HMOX1 expression?

Yes. Consistent with our mechanistic hypothesis, OAM treatment markedly attenuated HMOX1 overexpression in both models. In H/R-injured neurons and in hippocampal tissue following CPR, OAMs significantly reduced HMOX1 protein levels relative to untreated I/R groups (Fig. 6h,i). This downregulation parallels the normalisation of ferroptosis-related markers (e.g., Fe^{2+}, lipid peroxidation, GPX4/FTH1/ACSL4) and supports the notion that OAMs exert their neuroprotective effects, at least in part, by restraining pathological HMOX1 activation and thereby

limiting HMOX1-driven ferroptotic signalling.

(3) What is the potential mechanism for upregulating HMOX1?

Drawing on our data and recent literature, we propose that HMOX1 induction under H/R and CPR reflects the convergence of redox-sensitive transcriptional pathways and injury-associated stress signals: (i) NRF2-HMOX1 axis: H/R and I/R stress promote NRF2 activation and nuclear translocation, where NRF2 binds antioxidant response elements (AREs) in the HMOX1 promoter to drive transcriptional upregulation (*Neurotherapeutics, 2024, 21, e00444*). (ii) HIF1α stabilisation: I/R impairs Egln3-mediated degradation of HIF1α, leading to its accumulation and further enhancement of HMOX1 expression (*Redox Biol., 2024, 76, 103345*). (iii) Oxidative and inflammatory stress: Excessive ROS generation and elevated pro-inflammatory cytokines (e.g., TNF-α, IL-1β) during CA/CPR act as upstream stress signals that synergistically amplify HMOX1 expression as part of the canonical cellular defence response.

In this context, OAMs appear to blunt the magnitude of HMOX1 induction by alleviating oxidative stress and ferroptotic damage, thereby interrupting a positive feedback loop between HMOX1 activation, iron dyshomeostasis, and lipid peroxidation. This mechanistic interpretation has been incorporated into the revised manuscript (Lines 480-486; 718-722).

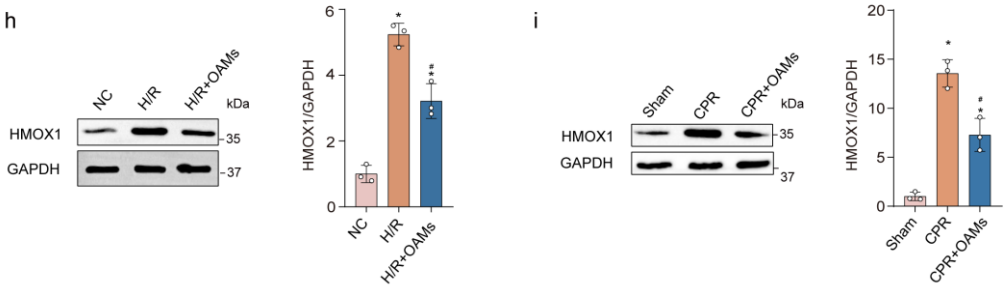

Fig. 6 h,i | h, Representative western blots (left) and quantification (right) of HMOX1 protein levels in HT22 cells under H/R with or without OAM treatment for 24 h (n = 3 biological replicates). Art-equivalent dose, 250 nM. **i**, Western blots (left) and relative expression levels (right) of HMOX1 in mouse hippocampal tissue 24 h after ROSC, following immediate post-ROSC administration of OAMs (n = 3 mice). Art-equivalent

dose, 5 mg kg^{-1}. Data are presented as mean ± SD. Statistical significance was determined by one-way ANOVA with Tukey's post hoc test (multiple groups). *P < 0.05 vs. NC or Sham; $^{\#}P$ < 0.05 vs. H/R or CPR.

Comment 13: In lines 430-431, the authors claim that HMOX1 overexpression "abolished" the cytoprotective effects of OAMs. However, while the data in Figures 8B-F show a statistically significant effect, the actual degree of rescue is minor. This suggests that OAMs have other protective mechanisms besides their effect on HMOX1, so the term "abolished" is an overstatement.

Author's response: Thank you for this insightful comment. We agree that describing the effect as "abolished" was an overstatement. While HMOX1 overexpression clearly increased neuronal vulnerability to H/R-induced ferroptosis, OAM treatment still conferred significant protection under these conditions. To more faithfully represent the data, we have revised the text to read (Lines 613-619):

" Even with HMOX1 overexpression, which worsened H/R-induced injury, OAMs still exhibited substantial anti-ferroptotic effects. Despite excessive HMOX1 activity, OAM treatment significantly counteracted the biochemical and mitochondrial abnormalities (Fig. 9a–f; Supplementary Fig. 17a, b) and largely normalised the expression of ferroptosis-related proteins, including the upregulation of GPX4 and FTH1 and the suppression of ACSL4 (Supplementary Fig. 17c–f)."

This wording clarifies that HMOX1 overexpression attenuates, but does not eliminate, the cytoprotective efficacy of OAMs. In line with the reviewer's point, we have also added to the Discussion that these findings imply the existence of additional HMOX1-independent protective mechanisms (e.g., broader antioxidant or anti-inflammatory actions of Art or OAMs), which will be an important focus of future mechanistic work (Lines 747-752):

"While our data highlight HMOX1-mediated ferroptosis as a key target of OAM therapy, HMOX1-independent antioxidant, mitochondrial, and anti-inflammatory effects of Art may also contribute (J. Int. Med. Res. 2021,49, 1–13; Mol. Med. Rep., 2018, 17, 6639-6646; Mol. Neurobiol., 2022, 59, 4718-4729). Thus, OAMs likely act

through combined HMOX1-centred ferroptosis suppression and broader cytoprotection (Intensive Care Med. 2021, 47, 1393-1414; Lancet. 2021, 398, 1269-1278). The relative contributions require further studies using Hmox1-deficient models or selective inhibitors."

Comment 14: In Figure 9A, treatment with the HMOX1 activator CoPPIX-Cl appears to reverse the therapeutic benefits of OAMs. To confirm the pathological role of increased HMOX1, I suggest the authors test whether an HMOX1 inhibitor (e.g., Zinc Protoporphyrin) can attenuate CPR alone-induced neuronal injury.

Author's response: Thank you for this insightful suggestion. In line with your recommendation, we performed additional *in vivo* experiments to evaluate whether pharmacological inhibition of HMOX1 is sufficient to attenuate CPR-induced brain injury. Zinc protoporphyrin (ZnPP), a selective HMOX1 inhibitor, was administered intraperitoneally 24 h before CA induction. ZnPP pretreatment significantly improved post-resuscitation neurological function (Supplementary Fig. 19a,b) and reduced serum NSE and S100β levels (Supplementary Fig. 19c,d). Moreover, ZnPP robustly suppressed CPR-induced ferroptotic injury, as evidenced by reduced hippocampal Fe^{2+} accumulation (Supplementary Fig. 19e) and MDA levels (Supplementary Fig. 19f), restoration of GSH (Supplementary Fig. 19g), and attenuation of hippocampal ROS accumulation (Supplementary Fig. 19h,i).

These findings support the conclusion that excessive HMOX1 activation is a key pathological driver of neuronal ferroptosis following CA/CPR and that HMOX1 inhibition confers significant neuroprotection *in vivo*. These additional data and the corresponding text have been incorporated into the revised manuscript (Lines 685-693).

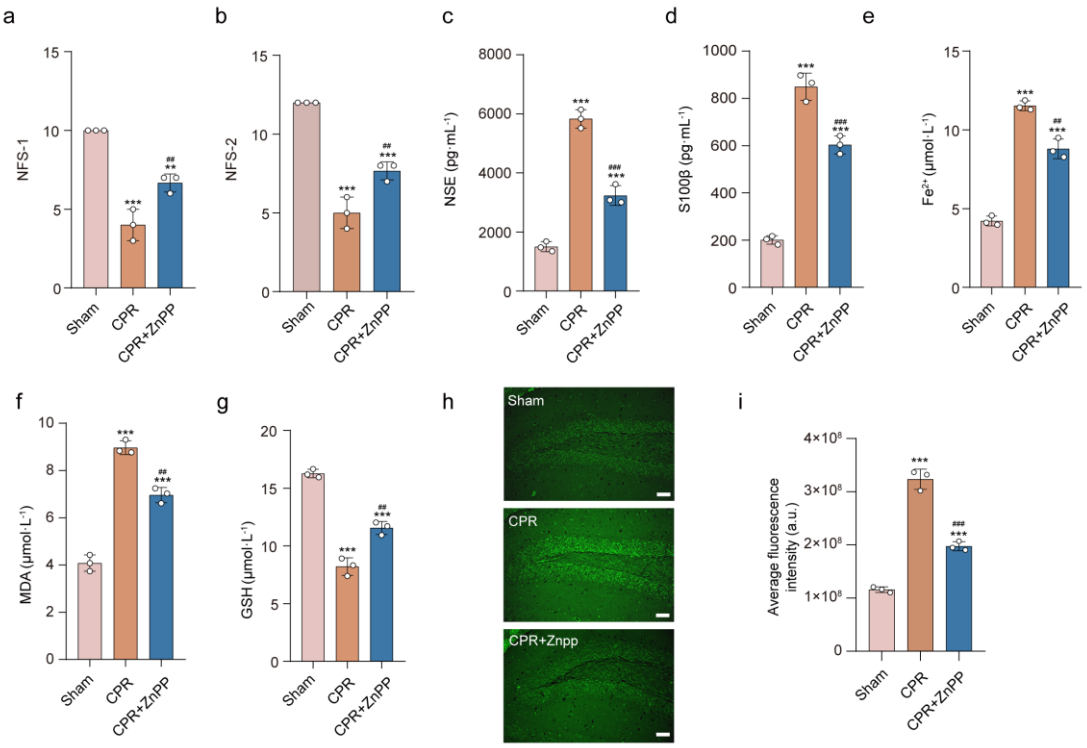

Supplementary Fig. 19 | HMOX1 inhibition alleviates post-resuscitation brain injury by suppressing ferroptosis *in vivo*. a, b, Neurological function scores (NFS-1, **a**; NFS-2, **b**) in CA/CPR mice receiving a single intraperitoneal (*i.p.*) injection of ZnPP 24 h before CA induction, assessed at 24 h post-ROSC. **c, d**, Serum levels of neuronal injury biomarkers NSE (**c**) and S100β (**d**) measured by ELISA at 24 h post-ROSC. **e–g**, Quantification of ferroptosis-related biochemical markers in hippocampal tissue from each group: cytosolic Fe^{2+} levels determined by ferrozine assay (**e**), MDA levels by TBA method (**f**), and GSH content by DTNB assay (**g**). **h, i**, Representative DCFH-DA fluorescence images (**h**) and quantitative analysis (**i**) of ROS levels in the dentate gyrus (DG) region of the hippocampus at 24 h post-ROSC. ROS signals are shown as green fluorescence. Scale bar, 100 μm. ZnPP-equivalent dose, 10 mg kg^{-1}. $n = 3$ mice per group. Data are presented as mean ± SD. Statistical significance was determined by one-way ANOVA with Tukey's post hoc test (multiple groups). $^{**}P < 0.01$, $^{***}P < 0.001$ vs. Sham; $^{\#\#}P < 0.01$, $^{\#\#\#}P < 0.001$ vs. CPR.

Comment 15: For the ROS staining shown in Figure 9Eiii, images should be taken from the same or adjacent tissue regions to ensure a valid comparison.

Author's response: Thank you for this valuable suggestion. We fully agree that consistent anatomical sampling is essential for valid comparison of ROS staining across groups. Accordingly, we have re-acquired the ROS images in Fig. 9e-iii (now Fig. 10e-iii) by imaging the same or immediately adjacent hippocampal regions under identical settings. We then re-performed quantitative analysis of ROS-associated fluorescence intensity using ImageJ (now presented in Fig. 10g). The updated data are fully consistent with our original findings and further support the conclusions drawn in the manuscript.

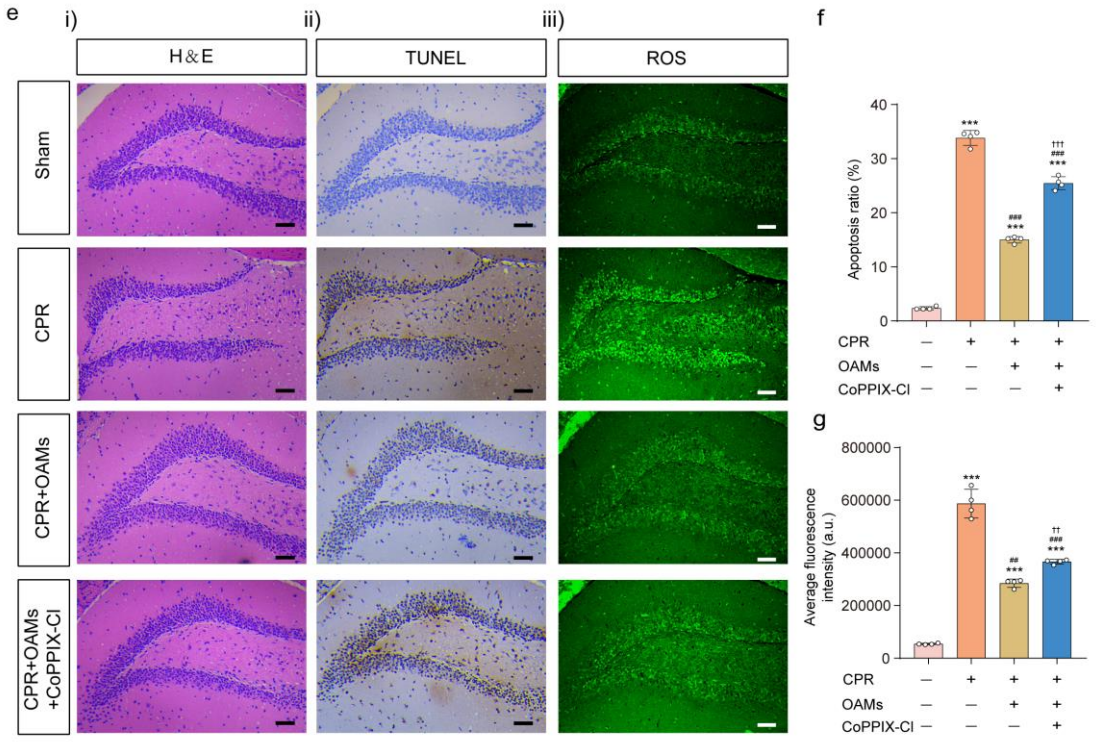

Fig. 10e-g | e, Histopathological assessment of hippocampal injury (n = 4 mice): (**i**) H&E staining; (**ii**) TUNEL assay; (**iii**) ROS visualisation in the DG region using DCFH-DA. Scale bar, 100 μm. **f, g**, Quantification of TUNEL-positive cells (**f**) and hippocampal ROS intensity (**g**) corresponding to panel **e-i** and **ii**, respectively. Art-equivalent dose, 5 mg kg^{-1}; CoPPIX-Cl-equivalent dose, 10 mg kg^{-1}. Data are presented as mean ± SD. Statistical significance was determined by one-way ANOVA with Tukey's post hoc test (multiple groups). ***P < 0.001 vs. Sham; $^{\#\#}P$ < 0.01, $^{\#\#\#}P$ < 0.001 vs. CPR; $^{\dagger\dagger}P$ < 0.01, $^{\dagger\dagger\dagger}P$ < 0.001 vs. CPR+OAMs.

Comment 16: Please ensure that all instances of "*in vitro*", "*in vivo*", and "*ex vivo*" are italicized throughout the manuscript.

Author's response: Thank you for your helpful suggestion. We have carefully reviewed the entire manuscript and ensured that all Latin phrases—*in vitro*, *in vivo*, and *ex vivo*—are now italicized throughout the manuscript.

Comment 17: In line 680, please state the pore size and catalog number of the transwell insert used for the trans-endothelial transport analysis.

Author's response: Thank you for pointing out this issue. We have now provided the full specifications of the Transwell inserts used for the trans-endothelial transport assays in the revised Methods section (Lines 891-893):

"bEnd.3 cells were seeded at a density of 5 × 10^5 cells per well on Transwell inserts equipped with a 0.4-μm pore size polycarbonate membrane (Corning, Catalog No. 3401, USA) and cultured with medium in both chambers refreshed every other day."

Comment 18: The immediate administration of the nanotherapy does not reflect clinical practice, where treatment is typically delayed. To address this, I suggest performing experiments where the OAMs are administered at progressively later time points after successful CPR to determine how long the therapy remains effective.

Author's response: Thank you for this important and clinically relevant suggestion. To better emulate clinical scenarios in which treatment is often delayed after ROSC, we performed additional *in vivo* experiments to define the therapeutic time window of OAMs following successful CPR. In these studies, OAMs were administered at delayed time points of 30, 60, and 120 min after CPR, and neurological function and biochemical markers of neuronal injury were evaluated. A progressive decrease in efficacy was noted as the delay to treatment increased (Supplementary Fig. 9). When given at 30 or 60 min post-CPR, OAMs retained strong neuroprotective efficacy, significantly improving neurological scores and lowering NSE and S100β levels. In contrast, administration at 120 min provided nearly no benefit, suggesting a clinically

actionable therapeutic window of up to 1 h post-resuscitation.

The new data and corresponding descriptions have been incorporated into the revised manuscript (Lines 374-381).

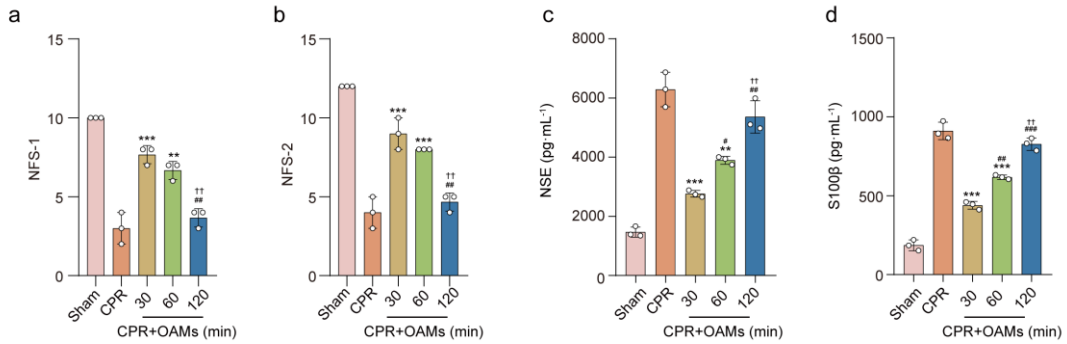

Supplementary Fig. 9 | Efficacy of delayed OAM administration following CA/CPR. a, b, Neurological function scores NFS-1 (**a**) and NFS-2 (**b**) assessed at 24 h after ROSC in mice receiving OAMs at delayed time points of 30, 60, or 120 min post-ROSC (n = 3 mice per group). Art-equivalent dose, 5 mg kg^{-1}. **c, d**, Serum concentrations of neuro-injury biomarkers neuron-specific enolase (NSE; **c**) and S100β (**d**) measured by ELISA at 24 h after ROSC in mice treated with OAMs at the indicated delayed time points (n = 3 mice). Art-equivalent dose, 5 mg kg^{-1}. Data are presented as mean ± SD. Statistical significance was determined by one-way ANOVA with Tukey's post hoc test (multiple groups). $^{**}P < 0.01$, $^{***}P < 0.001$ vs. CPR; $^{\#}P < 0.05$, $^{\#\#}P < 0.01$, $^{\#\#\#}P < 0.001$ vs. CPR+OAMs 30 min; $^{\dagger\dagger}P < 0.01$ vs. CPR+OAMs 60 min.

Comment 19: The manuscript's primary focus on HMOX1-mediated ferroptosis overlooks the fact that artesunate has broad antioxidant capabilities. The specificity of its action against HMOX1 is not fully established, meaning off-target effects could contribute to the therapeutic outcome. The manuscript must be revised to differentiate the neuroprotective effects of specific HMOX1 inhibition from the compound's other biological activities.

Author's response: Thank you for this insightful and important comment. We fully agree that artesunate (Art) possesses pleiotropic antioxidant and cytoprotective properties and that the specificity of its effects on HMOX1-mediated ferroptosis

requires careful discussion.

First, our mechanistic data—encompassing HMOX1 overexpression and knockdown, profiling of ferroptosis-related markers, ferritinophagy assays, and *in vivo* pathway validation—consistently support the HMOX1-ferroptosis axis as a central mediator of OAMs' neuroprotective effects. However, these studies do not exclude additional HMOX1-independent actions of Art. In particular, Art's broader activities, such as direct or indirect ROS scavenging, modulation of mitochondrial redox balance, and potential attenuation of pro-inflammatory signalling, may act in parallel with HMOX1 inhibition to mitigate neuronal injury after CA/CPR.

Second, we acknowledge that the current work does not quantitatively disentangle the relative contributions of (i) specific HMOX1 regulation versus (ii) non-specific antioxidant and cytoprotective effects of Art to the overall therapeutic benefit of OAMs. While the genetic manipulation experiments provide strong causal evidence that HMOX1 activity critically shapes ferroptosis severity under H/R and CPR, they do not establish that HMOX1 is the sole pharmacological target of Art in this context.

To address this point transparently, we have revised the Discussion and explicitly incorporated this issue as a limitation of this work as follows:

"While our data highlight HMOX1-mediated ferroptosis as a key target of OAM therapy, HMOX1-independent antioxidant, mitochondrial, and anti-inflammatory effects of Art may also contribute (J. Int. Med. Res. 2021,49, 1–13; Mol. Med. Rep., 2018, 17, 6639-6646; Mol. Neurobiol., 2022, 59, 4718-4729). Thus, OAMs likely act through combined HMOX1-centred ferroptosis suppression and broader cytoprotection (Intensive Care Med. 2021, 47, 1393-1414; Lancet. 2021, 398, 1269-1278). The relative contributions require further studies using Hmox1-deficient models or selective inhibitors."

We are grateful for this comment, which has helped us present a more balanced and rigorous interpretation of our findings. The corresponding text has been added to the revised Discussion (Lines 747-752).

Comment 20: The study confirmed the nanoparticles accumulate in neurons and

microglia. Expanding the investigation to include their effects on other crucial brain cells such as astrocytes, oligodendrocytes, and pericytes would provide a more complete understanding of the therapy's impact on the entire neurovascular unit and overall brain environment.

Author's response: Thank you for this thoughtful suggestion. In response, we performed additional *in vitro* studies to evaluate the impact of OAMs on astrocytes, oligodendrocytes, and pericytes under H/R conditions. Our results demonstrate that OAM treatment significantly improved the viability of all three cell types following H/R injury (Supplementary Fig. 7), even though the degree of protection was lower than that observed in neurons. These results imply that, apart from protecting neurons and microglia, OAMs exert broader cytoprotective effects on multiple components of the brain parenchyma, which might contribute to stabilizing the overall brain microenvironment after CA/CPR.

The supplementary data and discussion have been incorporated into the revised manuscript (Lines 352-358).

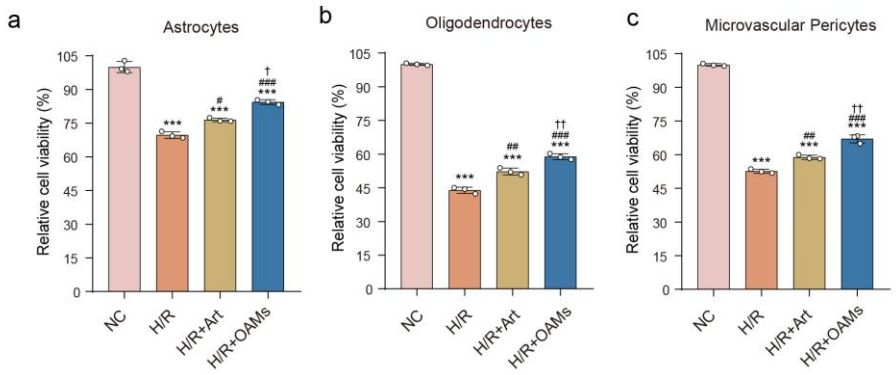

Supplementary Fig. 7 | OAMs preserve viability of multiple neurovascular unit cell types under H/R. Viability of primary astrocytes (**a**), oligodendrocytes (**b**), and brain microvascular pericytes (**c**) treated with OAMs for 24 h under H/R (n = 3 biological replicates). Art-equivalent dose, 250 nM. Data are presented as mean ± SD. Statistical significance was determined by one-way ANOVA with Tukey's post hoc test (multiple groups). $^{***}P < 0.001$ vs. NC; $^{\#\#}P < 0.01$, $^{\#\#\#}P < 0.001$ vs. H/R; $^{\dagger}P < 0.05$, $^{\dagger\dagger}P < 0.01$ vs. H/R+Art.

Comment 21: The study focuses on artesunate as the encapsulated drug, which limits generalizability of the delivery platform to other potential neurotherapeutics. More data on versatility might have strengthened the case for OPDEA micelles as a general nanocarrier.

Author's response: Thank you for this important and constructive comment. We agree that demonstrating the versatility of the OPDEA-PCL platform is essential to support its broader translational relevance beyond Art alone.

First, we note that OPDEA-PCL micelles are designed as a BBB-penetrant delivery module rather than an Art-specific formulation. The OPDEA corona enables AMT in both healthy and CA/CPR mice, providing receptor-independent, robust transport into the brain parenchyma and access to multiple resident cell types. This mechanism is, in principle, compatible with a wide range of CNS therapeutics for conditions where BBB impermeability is a key bottleneck.

To provide direct evidence of this versatility, we have encapsulated additional CNS-relevant small molecules with distinct indications and physicochemical profiles, including lomustine (LOM, an alkylating chemotherapeutic for glioma) and rasagiline (RAS, a clinically used neuroprotective agent for Parkinson's disease). OPDEA-PCL/LOM and OPDEA-PCL/RAS micelles displayed hydrodynamic sizes of 47.7 ± 1.0 nm and 62.7 ± 1.1 nm. Their drug loading contents (DLCs) were 6.2 ± 0.12% and 7.0 ± 0.7%, and drug loading efficiency (DLE) reached 67.0 ± 1.3% and 76.6 ± 0.7% (Fig. R1). These data indicate that OPDEA-PCL can effectively accommodate multiple small-molecule neurotherapeutics, supporting its application as a modular, widely applicable nanocarrier for CNS drug delivery.

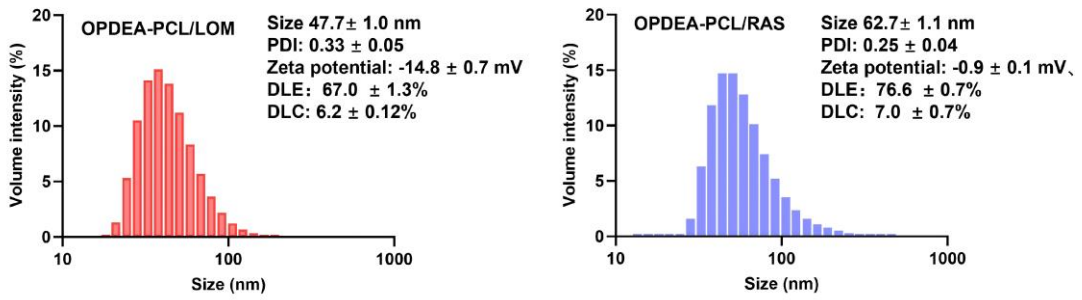

Fig. R1 | Hydrodynamic size, PDI, and zeta potential of OPDEA-PCL/LOM and OPDEA-PCL/RAS micelles as determined by dynamic light scattering (DLS), along with their drug loading contents (DLC) and drug loading efficiency (DLE) quantified by high-performance liquid chromatography (HPLC).

RESPONSES TO REVIEWERS' COMMENTS

Reviewer #1

I have read through the revised manuscript and the response letter. All my concerns have been well addressed and therefore I would recommend publication of the manuscript on Nature Communications.

Author's response: Thank you for positive recommendation for publication. We appreciate your time and effort throughout the review process.

Reviewer #2

The author has systematically responded to and revised the manuscript based on the reviewers' comments, significantly improving the rigor of the experimental design, the completeness of the mechanism derivation, and the standardization of the expression. The current version of the study has a novel concept. It achieves the penetration of the BBB by Art through OPDEA-based micellar carriers (OAMs) and targets the inhibition of HMOX1-mediated ferroptosis, providing an innovative and translation-potential treatment strategy for postiac-CA resuscitation brain injury. The research design is logically clear, the in vitro and in vivo data chains are basically complete, and the core conclusions are effectively supported. it has reached the publication level of the journal, and it is recommended to accept it after minor revisions.

Author's response: Thank you for your positive and constructive evaluation. We have addressed the remaining concerns as detailed below.

Comment 1: The authors only detected the neuroprotective effect and acute toxicity within 24 hours, without evaluating the long-term (e.g., 1 week, 4 weeks) neurological function recovery and the safety of long-term HMOX1 inhibition. Considering the requirements of clinical translation, it is recommended to supplement the long-term safety data or clearly state the limitations of the short-term experiment in the discussion.

Author's response: Thank you for your insightful comments. We fully recognize that long-term neurological recovery and thorough safety evaluation are essential to

successfully advancing a neuroprotective therapy into clinical practice. To address your concerns, we have revised the Discussion and incorporated these issues as limitations of this work as follows:

"Moreover, as post-resuscitation brain injury evolves across acute, subacute, and chronic phases, long-term behavioural assessments and histopathological analyses will be necessary to determine the durable benefits. Finally, given the essential roles of HMOX1 in haem metabolism and antioxidant defence, the long-term safety of sustained pathway inhibition, particularly with respect to cognition and neurogenesis, will require careful evaluation (Cell Mol. Life Sci., 2022, 79, 224; Redox Biol., 2021, 47, 102170)."

The corresponding text has been added to the revised Discussion (Lines 711-716).

Comment 2: It is recommended to polish the language of the article and simplify the long and complex sentences.

Author's response: Thank you for your helpful suggestion. We have carefully polished the language and simplified complex sentences to enhance readability.

Reviewer 3

The authors have addressed my questions, and I have no further inquiries.

Author's response: Thank you for your careful evaluation. We are pleased that all concerns have been addressed.